Deanship of Graduate Studies
Al-Quds University

Evaluation of the Application of Orthopedic Metal Artifact Reduction and Iterative Reconstruction Algorithms in CT Imaging of Hip Prostheses

Omarah Abd Alqader

M.Sc. Thesis

Jerusalem- Palestine

1442/2021

Evaluation of the Application of Orthopedic Metal Artifact Reduction and Iterative Reconstruction Algorithms in CT Imaging of Hip Prostheses

Prepared By: Omarah Naser Saed Abd Alqader

B.Sc. of Medical Imaging, Al-Quds University/ Palestine.

Supervisor: Dr. Hjouj Mohammad

A Thesis Submitted in Partial Fulfillment of Requirements for the Degree Master of Medical Imaging Technology/ Functional Imaging Track/ Faculty of Health Professions/ Al-Quds University

Jerusalem- Palestine

1442/2021

Al-Quds University
Deanship of Graduate Studies
Faculty of Health profession
Medical Imaging Technology

Thesis Approval

Evaluation of the Application of Orthopedic Metal Artifact Reduction and Iterative Reconstruction Algorithms in CT Imaging of Hip Prostheses

Prepared by: Omarah Abd-Alqader

Registration Number: 21811949

Supervisor: Dr. Mohammad Hjouj

Master Thesis Submitted and Accepted: 28 / 05 / 2021

The name and signatures of the examining committee members are as follows:

1- Head of Committee:	Dr. Mohammad Hjouj	Signature:
2- Internal Examiner:	Dr. Hussein ALMasri	Signature: Hussein ALMasri
3- External Examiner:	Dr. Muntaser Al Saied	Signature:

Jerusalem-Palestine

1442/2021

Dedication

This Research is Dedicated to

My Dear Parents, Family, Instructors, and Colleagues

Declaration:

I certify that this thesis submitted for the degree of Master is the result of my research, except where otherwise acknowledged, and that this study (or any part of the same) has not been submitted for a higher degree to any other university or Institution.

Omarah Naser Abd Alqader

Signed: 

Date: 28/05/2021

ACKNOWLEDGEMENT

May Allah, the Founder of the world, have mercy on us all. Special thanks are given to Dr. Mohammad Hjouj for his sponsorship of my studies, for his endurance and inspiration. Also, I would like to send special thanks to Dr. Mohammad Aljamil, for his assistance in building the phantom. Finally, I would like to express my appreciation to Dr. Fawaz and Hamzah Arjah, and my beloved wife for their assistance.

Omarah N. Abd Alqader

Abstract

The CT imaging of metal hip prosthesis causes metal-related artifacts reducing the overall image quality and clinical value of CT. This study aims to an evaluation of using orthopedic metal artifact reduction (O-MAR) technique and iterative model-based reconstruction (IMR) in CT imaging of bilateral total hip prostheses in a pelvis phantom. The fabricated pelvis phantom has four major components, pelvis bones, muscle, fat, and vascular structures, and was made using different concentrations of respectively calcium sulfate, bee wax, agarose powder, and Iohexol. Two types of hip prosthesis were used total hip and Austen Moore prosthesis. Different types of algorithms, filtered back projection (FBP), iDose^4, and IMR with different Kilo-Voltage peak (kVps) settings at 80, 100, 120, and 140, combined with O-MAR were applied on this phantom. The image quality criteria were CT number, noise, and signal to noise ratio (SNR) and were analyzed by five regions of interest (ROIs), while regions R1 and R5 were the primary focusing. The five RIOs representing the following anatomy (right common iliac artery, left common iliac artery, right gluteus medius muscle, fat, and urinary bladder) respectively from R1 – R5. Without the prosthesis, results showed that IMR resulted in lower CT number, noise values, and increased SNRs relative to FBP and iDose^4 for regions R1-R5. With the prosthesis, O-MAR improved CT-number precision for region R1 by 49% and 83% for FBP and IMR ($p<0.05$), relative to iDose^4 by 57% without any significant changes at ($p<0.05$). For region R5, O-MAR improved CT-number precision by 81%, 89%, and 92% towards baseline values for respectively FBP, iDose^{4,} and IMR ($p<0.05$). Also, O-MAR was most efficient in minimizing noise when integrated with IMR with corrections in the noise in R5 with 79 %, 90 %, and 92 % for respectively FBP, iDose^{4,} and IMR ($p<0.05$). . Additionally, O-MAR was most effective in correcting SNR deviations when integrated with IMR with absolute SNR corrections in region R5 with 29 ± 1 and 43 ± 4 for FBP and IMR ($p<0.05$), compared to iDose^4 by 37 ± 7 without any significant changes ($p>0.05$). For region R1, O-MAR improves SNR corrections by 5 ± 1, 23 ± 5, and 42 ± 9 for respectively FBP, iDose^{4,} and IMR ($p<0.05$). O-MAR paired with IMR revealed an HU correction for region R5 of 90%, 90%, 93%, and 93% for respectively 80, 100, 120, and 140-kVp results. Noise was corrected for with 92%, 91%, 92% and 92% for respectively 80, 100, 120 and 140-kVp results. SNR corrections were 37%,

38%, 46% and 52% for respectively 80, 100, 120 and 140-kVp results. For region R1, O-MAR combined with IMR showed an average HU correction of 90%, 68%, 81%, and 93% for respectively 80, 100, 120, and 140-kVp results. Noise was corrected with 89%, 88%, 90% and 89% for respectively 80, 100, 120 and 140-kVp results. SNR corrections were 55%, 42%, 38% and 34% for respectively 80, 100, 120 and 140-kVp results. In conclusion, O-MAR decreases the appearance of metal artifacts using iDose^4 and is most efficient in severe artifacts when used in combination with 140-kVp and IMR. CT imaging of a bilateral total hip prosthesis phantom, using IMR together with O-MAR increases image quality by significantly minimizing metal artifacts, reducing noise, and enhancing CT number and SNR.

Table of Contents

List of Tables

Page

List of Figures

Page

List of Equations

Definitions and Abbreviations:

ADMIRE: Advanced modeled iterative reconstruction: is the latest innovation in iterative reconstruction introduced by Siemens, which uses iterative reconstruction from the raw data domain in combination with noise reduction in the image space in a hybrid manner. It applies statistical modeling in the raw data domain, followed by back projection, application of the statistical model in the image domain (regularization), and forward projection. The resulting pseudo raw data are compared to the measured data and iteratively reinserted into the loop afterward.

AIDR: Adaptive iterative dose reduction: is a hybrid reconstruction algorithm, introduced by Toshiba, which statistical model in combination with an imaging model that is used on the raw data to reduce noise and artifacts. The iterations are executed in image space only, where edge preservation and smoothing are performed. The corrected image is blended with the initial image (from the raw data) to keep the noise granularity. There are three different levels of iteration with different iterative strengths: mild, standard, and strong.

AIDR 3D: Adaptive iterative dose reduction three-dimension: is a hybrid reconstruction algorithm, introduced by Toshiba, incorporating raw data domain and image domain noise reduction techniques that reduce noise and artifacts while preserving a high level of spatial resolution. AIDR 3D ensures automated dose reduction based on patient size, a user-determined target level of image quality, and noise reduction capabilities.

ASIR: Adaptive statistical iterative reconstruction: A hybrid iterative reconstruction algorithm introduced by GE uses a blend of filtered back-projection images with iterative reconstruction images in the raw data domain to reduce the image noise. ASIR performs a hybrid iterative process of mathematical and statistical modeling to identify and selectively reduce the noise of an image.

ASIR-V: Adaptive statistical iterative reconstruction combined with Veo. ASIR-V combines the speed of ASIR with additional capabilities from Veo, GE's full model-based iterative reconstruction technology. By applying more advanced modeling and optimization technologies in projection- and image-space as part of the iterative

reconstruction process, ASIR-V provides dose reduction well beyond that of ASIR, while maintaining low-contrast detectability, like Veo.

$CaSo_4$: Calcium sulfate: is the inorganic compound with the formula $CaSo_4$ and related hydrates and is a naturally occurring calcium salt. It is commonly known in its dihydrate form, a white or colorless powder called gypsum.

CNR: Contrast to noise ratio: a measure of image quality based on contrast rather than the raw signal. CNR is similar to the metric signal-to-noise ratio but subtracts a term before taking the ratio.

CT: Computed Tomography: Sometimes called computerized tomography or computed axial tomography (CAT), is an imaging modality that utilizes x-ray photons for image production, with digital reconstruction. The CT scanner essentially consists of an x-ray tube and detectors. The x-ray tube produces an x-ray beam that passes through the patient. This beam is captured by the detectors and reconstructed to produce cross-sectional images of the body. Each cross-sectional image represents a "slice" of the person being imaged. These cross-sectional images are used for a variety of diagnostic and therapeutic purposes.

CTDI: CT-dose index: is an estimation of the average dose during the CT scan volume to a standardized phantom.

Detector: A device sensitive to radiation that produces a current or voltage pulse that may or may not correspond to the energy deposited by an individual photon or particle.

DICOM: Digital Imaging and Communications in Medicine: is a standard that establishes rules that allow medical images and associated information to be exchanged between imaging equipment from different vendors, computers, and hospitals.

Dose: The radiation delivered to the whole human body or a specified area or organ of the body. This term is used frequently in whole-body counting applications.

Dose Modulation: Technique automatically increases the mAs in the body part with the greatest attenuation and decreases mAs in the body part with lower attenuation. Depending on the amount of attenuation on the scout image.

FIRST: Forward projected model-based iterative reconstruction solution. Is a true, fully implemented model-based iterative reconstruction algorithm, introduced by Toshiba, meaning a forward projection step is performed for every iteration. FIRST operates by formulating an initial "guess" at an image result based on the measured raw projection data acquired during the scan. This initial guess is called a "seed image." The seed image is then forward projected in a process that mathematically mimics the process of data acquisition to create a new set of synthesized projection data. This new set of synthesized projections is then fed into the iterative reconstruction loop.

Frequency Splitting: This is an extension to the metal artifact reduction methods that recovers noise texture and anatomical details in the close vicinity of metal.

Helical (Spiral) Scanning: Many recent technical developments allowed the introduction of continuous acquisition scanning most often called helical or spiral scan. This type of scan, which allows continuous table movement and continuous X-ray tube rotation, would lead to less scan time and less radiation dose for the patient.

HU: Hounsfield units or CT numbers. A dimensionless unit is universally used in computed tomography (CT) scanning to express CT numbers in a standardized and convenient form. Hounsfield units are obtained from a linear transformation of the measured attenuation coefficients.

iDose^4: Fourth-generation hybrid iterative reconstruction algorithm introduced by Philips.

IMR: Iterative model-based reconstruction. A full iterative reconstruction technique was introduced by Philips.

IMAR: Iterative metal artifact reduction. A metal artifact reduction technique was introduced by Siemens.

IR: Iterative reconstruction. Is an alternative image reconstruction method that allows imaging at lower doses while maintaining image quality comparable to routine dose filtered back projection.

IRIS: Iterative reconstruction in image space. Iterative reconstruction algorithm, introduced by Siemens, that uses an initial Filtered back-projection algorithm to

reconstruct the images, in a second moment noise is removed in iterative steps: this process should preserve the spatial resolution obtained during the first traditional reconstruction cycle.

kVp: Kilo-Voltage peak. It is the X-ray photons energy.

MAR: Metal artifact reduction. Algorithms are used to improve CT image quality in patients with metalware.

MARIS: Metal artifact reduction in image space. It is based on segmentation, forward projection, and interpolation with two-compartment physical modeling. The technique was introduced by siemens and was initially introduced to improve image quality for radiation therapy planning.

mAs: milliAmpiresecond. Is the x-ray tube current milliAmpere (mA) per scan time (s), which is represented the amount of radiation X-ray photons per second.

MBIR: Model-based iterative reconstruction. Is a fully iterative reconstruction using both forward and backward reconstruction steps. This algorithm also models system statistics and system optics, allowing fewer approximations and less error propagation during the reconstruction steps, compared with a filtered back-projection algorithm.

mGy: miliGray. The SI unit of absorbed dose. Defined as one joule per kilogram of absorbing medium.

NMAR: Normalized metal artifact reduction. The algorithm uses different steps for metal artifact reduction. From the original raw data, an uncorrected image is reconstructed. By thresholding, the metal image and the prior image are obtained. Forward projection yields the corresponding sinograms. The original sinogram is then normalized by dividing it by the sinogram of the prior. The metal projections determine where data in the normalized sinogram are replaced by interpolation. The interpolated and normalized sinogram is denormalized by multiplying it with the sinogram of the prior image again. Reconstruction yields the corrected image.

Noise: Quantum mottle. Is an unwanted change in pixel values in an otherwise homogenous image. Often noise is defined loosely as the grainy appearance on CT imaging.

Partial volume effects: Effects occur where multiple tissues contribute to a single voxel, resulting in a blurring of intensities at tissue boundaries.

Pitch: Estimate by the table movement (increment distance) per one full rotation of the X-ray tube divided by the width of the X-ray beam.

Photon: In quantum theory, light is propagated in discrete packets of energy called photons. The quantity of energy in each packet is called a quantum.

PMMA: Polymethyl methacrylate. Also known as acrylic or acrylic glass, is a transparent and rigid thermoplastic material widely used as a shatterproof replacement for glass. PMMA has many technical advantages over other transparent polymers (PC, polystyrene, etc.), a few of them include high resistance to ultraviolet light and weathering, excellent light transmission, and unlimited coloring options.

Radiation: The emission or propagation of energy through matter or space by electromagnetic disturbances which display both wave-like and particle-like behavior. Though in this context the "particles" are known as photons, the term radiation has been extended to include streams of fast-moving particles. Nuclear radiation includes alpha particles, beta particles, gamma rays, and free neutrons emitted from an atomic nucleus during decay.

Reconstruction Slice Thickness: Increasing the slice thickness improves the signal-to-noise ratio due to an increase in the number of photons for each voxel and disturbs spatial resolution.

ROIs: Regions of interest.

Rotation Time: Gantry rotation time describes the required time for the X-ray tube to rotate 360^{o}.

SAFIRE: Sinogram affirmed iterative reconstruction, is a unique CT iterative reconstruction algorithm that uniquely allows for up to 60% lower radiation dose in CT examinations without compromising image quality.

Scattering: A process that changes a particle's trajectory. Scattering is caused by particle collisions with atoms, nuclei, and other particles or by interactions with electric

or magnetic fields. If there is no change in the total kinetic energy of the system, the process is called elastic scattering. If the total kinetic energy changes due to a change in internal energy, the process is called inelastic scattering. See also backscattering.

SEMAR: Single-energy metal artifact reduction. Is a raw data-based technique, introduced by Toshiba, that incorporates the gradient correction features of iterative reconstruction with clinically reasonable reconstruction times.

SMAR, MARS: Smart metal artifact reduction. Metal artifact correction technology, introduced by GE health care, uses an automated, three-stage projection-based process to help improve the quality of CT data within the projection space, rather than in image space. This projection space correction leads to images that are consistent with the uncorrected image and of exceptional image quality.

SNR: Signal to noise ratio. is a generic term that is equal to the ratio of the average signal intensity over the standard deviation of the noise.

Streaks: In very heterogeneous cross-sections, dark bands or streaks can appear between two dense objects in an image. They occur because the portion of the beam that passes through one of the objects at certain tube positions is hardened less than when it passes through both objects at other tube positions. This type of artifact can occur both in bony regions of the body.

THA: Total hip arthroplasty. Is one of the most cost-effective and consistently successful surgeries performed in orthopedics. THA provides reliable outcomes for patients suffering from end-stage degenerative hip osteoarthritis, specifically pain relief, functional restoration, and overall improved quality of life.

The 3Rs: Stand for Replacement, Reduction and Refinement – are embedded into the legislation and guidelines governing the ethics of animal use in experiments.

Ti-6Al-4V: Titanium-aluminium-vanadium alloy. An alloy that contains a mixture of titanium and small amounts of aluminum and vanadium, typically 6% and 4% respectively, by weight and has been frequently used as a surgical implant.

Undersampling: The number of projections used to reconstruct a CT image is one of the determining factors in image quality. Too large an interval between projections

(undersampling) can result in misregistration by the computer of information relating to sharp edges and small objects. This leads to an effect known as view aliasing, where fine stripes appear to be radiating from the edge of, but at a distance from, a dense structure.

USA: United State of America.

Veo: A full iterative reconstruction or model-based iterative introduced by GE. Veo is a fully iterative method working in the raw data domain, which takes not only the data statistics into account but also the geometry of the machine itself by considering the voxel volumes of the scanned object, the focal spot size, the active area size of the detector, etc. With Veo, lower noise and higher resolution can be achieved within a single image.

Window Level: The window level or window center determines the center point of the window width.

Window Width: The window width determines the number of CT numbers displayed on a specific image.

X-Ray: A penetrating form of electromagnetic radiation emitted during electron transitions in an atom to a lower energy state; usually when outer orbital electrons give up some energy to replace missing inner orbital electrons.

Chapter 1

Introduction

1.1 Background of the Study

Computed tomography (CT) is usually described as a breakthrough medical imaging technique in medicine since its launch in the early 1970s. CT consists of a rotating X-ray tube and detectors in conjunction with a computer that processes the internal organs and structures and creates cross-sectional and three-dimensional images. In comparison to X-ray radiography, it provides a high-quality image, contrast, and more details that can cover wide regions of the patient's body. The cost of the CT examination is fair and this procedure is simple and easy to execute [1]. The CT scan is extremely helpful, as several various kinds of tissue such as lungs, heart, bones, soft tissues, muscles, and blood vessels can be viewed simultaneously [2]. With constant and wide enhancements in efficiency, resolution, accuracy, and speed the number of CT scanners is growing drastically [3]. However, there is an increasing concern regarding the risks of such radiation exposure. Radiation-induced cancer is a probabilistic (stochastic) effect. CT is correlated with high radiation exposure increasing the risk of developing cancer, although even lower doses of radiation might cause carcinogenesis [2].

The number of joint replacement procedures has gradually risen in the last ten years due to population aging and the effectiveness of such implants in pain management and joint function reconstruction [1]. Hip replacement is the second most frequent joint replacement operation, (300,000 hip arthroplasties performed in the USA, and more than 1 million per year worldwide) [4], with a growing number of surgical procedures with the elderly population [1]. The diagnosis of prosthesis-related complications is mostly based on standard radiography. However, if a clinical X-ray initial analysis is not confirmed, the use of other imaging methods is required [1]. CT has been used for a long to make a thorough evaluation of hip replacements (implant parts, bone and/or cement interfaces, bone stock, soft tissue), which have been in use for many years for evaluating replacement joints [1]. The CT imaging of metal hip prosthesis causes metal-related artifacts. These metal artifacts are caused by a combination of multiple mechanisms, including photon starvation, beam hardening, scattering, partial volume effects, under-sampling, and patient motion [5,6].

The phrase artifact in CT has represented any systemic disparity between the Hounsfield units (HU) on the reconstructed image and the true attenuation coefficient of the object. CT Images are generally more sensitive to artifacts than conventional X-rays since the image is reconstructed on the order of something of a million individual calculations from the detector. The reconstruction methodology considers that each of these measurements is standard, so any fault in measurement is generally reflected as an error in the image that was reconstructed [7]. Metal-related artifacts have since the early days reduced the diagnostic value of CT images [5]. Artifacts caused by metallic implants, such as dental fillings, surgical clips, coils, cables, and orthopedic hardware, appear as bright and dark streaks through the reconstructed image [8]. This condition also leads to the reduced image quality of the surrounding tissue as well as of the metal implant itself. Relevant anatomical features are often entirely concealed by artifacts, which raises the risk of losing relevant findings.

In the past, many cases of solutions had been used in hospitals to minimize metal artifacts nevertheless, they were almost inadequate. One solution is increasing kilo-Voltage peak (kVp), however, it could only decrease metal artifact deterioration to a smaller level and would not enhance the imaging of larger implants such as hip prosthesis [8] Elevated tube current, on the other hand, can result in a higher dose of radiation to the patient and would not have a significant impact on image quality either [8]. Strategies such as gantry tilting, the use of lower attenuating materials in implants, reducing overall collimation, and the use of a soft reconstruction kernel instead of a bone kernel [9] to eliminate metal artifacts can only be feasible in particular circumstances and are successful to a restricted extent [10].

Metal Artifact Reduction (MAR) approaches concentrate on resolving these metal artifacts, either by minimizing the actual origin of the artifact or by fixing artifacts in image data or projection data. Despite these advancements in science, artifacts are still not fully conquered. Artifacts caused by metal implants arise at varying stages of intensity owing to the number of metals, forms and proportions utilized [9]. In the last few decades, significant changes have been made to both the acquisition of image and reconstruction, leading to a growth in CT imaging [9]. Filtered Back Projection (FBP) has been the industry standard for the reconstruction of CT images for centuries [11]. FBP is a sub-optimal algorithm selection for improperly sampled data or where noise amplifies the image signal. These circumstances can arise in low-dose or tube-power-limited acquisitions. FBP, whereas fast

and reasonably stable at regular radiation doses, is sensitive to image noise and artifacts resulting in non-diagnostic images at exceedingly low doses [11]. There are many explanations for the appearance of streak artifacts in FBP, such as imprecise beam hardening correction and photon starvation [11,12].

Classical back-filtered projection is replaced by iterative image reconstruction algorithms that allow the patient dose to be lowered and better suppress image artifacts [13]. Iterative reconstruction (IR) or so-called hybrid reconstruction techniques are blending techniques that combine IR images with FBP [14]. IR techniques properly handle noise at very low signal levels and thus reduce the noise and artifacts present in the final reconstructed image. This results in a considerable increase in image quality at any given dose. Using IR techniques, noise can be managed for high spatial resolution reconstruction, thereby providing high-quality, low-contrast, and spatial resolution within the same image [11]. iDose^4 is a fourth-generation hybrid IR algorithm introduced by Philips Healthcare (Cleveland, OH). iDose^4 provides an innovative solution in which iterative processing is performed in both the projection and image domains [15]. On the other hand, model-based iterative reconstruction (MBIR) techniques are more capable of handling increased detector noise levels at a reduced dose compared with the standard reconstruction technique, FBP, and IR techniques as it incorporates data statistics, image statistics, and system models. Using MBIR, images are being reconstructed at decreased levels of radiation at minimal levels of noise [16]. Also, MBIR decreases the volume of artifacts and allows for equivalent or greater visualization of bone-metal interfaces, and facilitates the evaluation of soft tissue around implants relative to FBP 16. Yasaka et al. (2013) observed that streak artifacts had been decreased using MBIR [17]. Also, de Kuya et al. (2017) reported that MBIR further decreases the size of artifacts and that MBIR enables for an equivalent or greater visibility of the bone-metal interface and increases the evaluation of soft tissue around implants relative to FBP [18]. Philips' iterative model-based reconstruction (IMR), is a full iterative reconstruction technique [19]. Furthermore, IMR does not involve blending with FBP such as hybrid iterative reconstruction techniques, which results in substantially improved image quality [20].

Besides, metal hardware impairs the diagnostic performance of CT for musculoskeletal imaging. Serious metal artifacts in the case of THA are primarily caused by severe photon starvation and influence an accurate diagnosis of prosthesis-related soft tissue and bone abnormalities [1]. Some of the currently available MAR techniques have previously

been studied in a variety of various clinical examples, ranging from artifacts formed by tiny metal objects such as dental fillings or screws to larger implants such as hip prostheses [10]. Li et al. [21] researched the implementation of a commercially available MAR algorithm in radiotherapy treatment planning and reported that it enhanced CT number precision and shape visualization in CT images of orthopedic implants. However, an increase in CT precision has been seen to have no major therapeutic effects on photon dose measurements.

There are several Software manufacturers are using iterative MAR algorithms as shown in Table 1.1. MAR technology from GE (Smart MAR: MAR or MARS), Toshiba (Single-Energy MAR: SEMAR), Siemens (MAR in Image Space: MAR and Iterative MAR: IMAR), Philips (Orthopedic MAR: O-MAR), and are all focused on in-painting, with the previous image, frequency splitting or a mixture of these strategies. Nevertheless, comprehensive vendor-specific MAR methodologies remain unknown [9]. Wagenaar et al. (2015) studied many commercial MAR strategies in anthropomorphic head and neck phantoms. In addition to the MAR technique of each scanner, the reconstructed metal artifact scans were reconstructed using the metal deletion technique (MDT). This technique was developed by Boas et al. (2011) and is based on reconstructed images instead of sinogram data [1]. HU errors were better minimized by O-MAR, followed by SMAR and Siemens' metal artifact reduction in image space (MARIS). The commercial Philips' O-MAR algorithm is an iterative projection adjustment approach specially developed for CT imaging of large metal orthopedic implants to decrease metal artifact [22]. O-MAR post-processes algorithm can increase the overall performance of iDose[4] and IMR [22]. Recently, a phantom study showed that O-MAR significantly reduces metal artifacts when combined with iDose[4] and IMR, which are Philips' proprietary (IR) technique and (MBIR) respectively [6]. Using O-MAR, HUs are corrected toward baseline levels, and contrast-to-noise-ratios (CNRs) are boosted [6].

Table 1.2: MAR algorithms, and (model-based) iterative reconstruction techniques of different Manufacturers [9].

Manufacturer	MAR algorithm	(Model-based) Iterative reconstruction techniques
Siemens	MARIS, IMAR	IRIS (1-5) Safire (1-5) Admire (1-5) *
Philips	O-MAR	iDose^4 (1-7) IMR (1-3) *
GE	SMAR, MARS	ASIR (0-100%), ASIR-V (0-100%) Veo*
Toshiba	SEMAR	AIDR (Mild, standard, strong), AIDR 3D (Mild, standard, strong) FIRST (Mild, standard, strong) *

*MBIR: Model-based iterative reconstruction.

1.2 Problem Statement

The CT imaging of metal hip prosthesis causes metal-related artifacts. Moreover, the overall image quality and clinical value of CT are distorted as these artifacts obstruct the accurate evaluation of bone-metal interfaces, vessels, bone, and soft tissue near to metal hardware.

Another risk of CT is radiation exposure. Decreasing radiation dose in patients with unilateral or bilateral hip prostheses may be an additional concern since the effect of the metal decreases the number of photons reaching the detector. The traditional way of modifying scanning parameter–related factors or using the classical filtered back-projection algorithm is a sub-optimal solution for handling these metal artifacts and at the cost of increased patient dose [23].

1.3 Justification

The phantom preparation is simple, low cost, reusable, and takes about 84 hours for preparation. The new phantom, with and without a total hip prosthesis, can provide the

researchers with a wide range of research experiments considering the Replacement, Reduction, and Refinement (3Rs).

Patients with hip implants and metal fixation hardware can benefit from the potential increase in image quality because of the minimization of metal artifacts and utilizing (model-based) iterative reconstruction can help. Also, analyzed with fewer distorting artifacts and noise levels eventually increasing CT's diagnostic value. Therefore, medical choices may be taken with more certainty concerning soft tissue and bone pathology and dysfunction of the prosthetic hardware. Furthermore, reducing CT radiation could reduce the incidence of radiation-induced hazards. By properly understanding the cause of metal artifacts, the variations in the severity of metal artifacts, and the ways to minimize artifacts, imaging procedures may be modified from acquisition to reconstruction and display parameters for particular hardware. The adjustment of these parameters is of particular significance in musculoskeletal CT imaging involving metal hardware.

Significant advancements in the image reconstruction process have been made over the last decades, from standard filtered back-projection to iterative reconstruction and model-based iterative reconstruction. By using model-based iterative reconstruction and MAR software, image quality may be improved with reduced metal artifacts, lower noise values, and radiation dose [9].

1.4 Study Objectives

This study has multiple goals:

1. To evaluate the effect of using different types of algorithms (FBP, iDose[4,] and IMR) with different kVps setting at 80, 100, 120 and 140, in imaging pelvis phantom with and without bilateral hip prosthesis.

2. To demonstrate the effectiveness of the orthopedic metal artifact reduction technique in improve image quality and reduce metal artifact in CT imaging of hip prostheses.

1.5 Study Hypothesis

Using of orthopedic metal artifact reduction technique and iterative model-based reconstruction will improve image quality while reducing CT radiation dose in patients with bilateral hip prostheses.

Chapter 2

Literature Review

This chapter presents some causes of metal artifacts and some approaches to metal artifact reduction strategies. Also, reviews some literature, published studies, and researches on metal artifact reduction techniques and display different methodologies that were used to reduce these artifacts.

2.1 CT Metal Artifacts

Metal artifacts are prominent in clinical images and are induced by various processes, most notably beam hardening, scattering, photon starvation, noise, and edge effects [9] Figure 2.1. These inputs cause corrupt data in order to be used to reconstruct near-metallic tissue, resulting in an incorrect tissue representation. As a result, depending on the amount and structure of the metal in situ, studying tissue around metal is unreliable and often impractical. These artifacts reduce the value and diagnostic accuracy of CT in bones, bone-metal interfaces, vessels, and soft tissue structures.

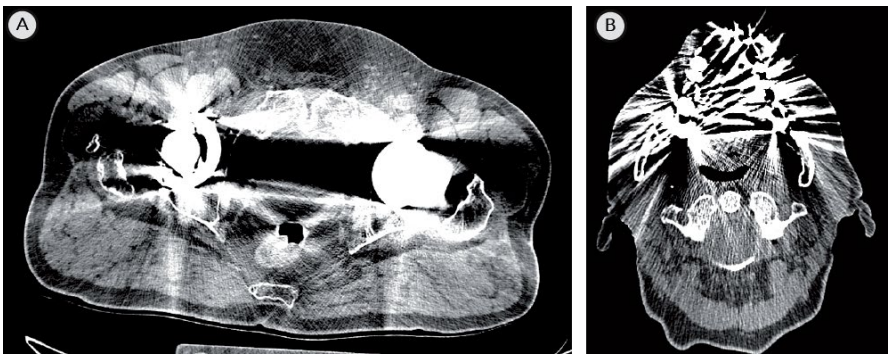

Figure 2.2: Metal Artifact: (A) Beam hardening, photon starvation, and scattering produce dark lines between the hip prosthesis. (B) A mixture of these artifacts from dental implants composed of heavy molecular weight metals [9].

Beam hardening occurs in polychromatic x-ray beams as the total beam intensity rises (hardens) as lower-energy photons become more readily absorbed by an object. This effect is more pronounced in the presence of materials with a high atomic number, such as metals, which attenuate low-energy x-rays dramatically creating dark streaks among highly attenuating items [9]. The attenuation of residual photons with a higher

average intensity is dominated by Compton scattering, which shifts the x-ray direction and causes the emitted photons to penetrate the detector of the central axis of the incident beam [24]. Both beam hardening and scattering result in further photons hitting regions of the detector where they will not usually be, contributing to misinterpretation of the attenuation coefficient [24]. Scatter causes photons to change their track. However, the reconstruction algorithms assume a straight line between the tube and the detector. Consequently, the scattered photons end up in the wrong detector. The scattered photons contribute to the calculated amplitude which contributes to an underestimation of the absorption and hence to dark streaks in the image, while an overestimation of the absorption causes white streaks [9].

Noise or variations in a standard content CT number are not normally treated as an artifact even if it affects the final image. These variations can occur on CT images as haziness and are induced by the small photon numbers with which an image forms [9]. However, metal artifacts in CT are often influenced by noise. Since photon flux calculated by CT detectors roughly represents a Poisson distribution, low photon counts would lead to higher proportional statistical errors in related detector regions [24]. Furthermore, detector electrical noise influences measurements at very low signal values. Since these errors are spontaneous, they appear in the image as a small dark and light streak [24]. Photon starvation may represent high-density metals and metals with a large atomic number. This results in low photon numbers and higher noise levels and loss of projection data. When no photons are observed at all, the background signal of the detector raises the noise value as well. This causes dark streaks of totally white metal in the final reconstructed image [9]. At rough edges of high or low absorbing tissues, edge effects may be detected. Edge effects often result in light or dark lucent streaks, reducing the corresponding grey value around long edges [9].

2.2 Metal Artifact Reduction Strategies

2.2.1 Adjustment of the Traditional Acquisition and Reconstruction

Standard methods for reducing the volume of metal artifacts include increasing the kVp and mAs. More photons can penetrate the detector as the average photon intensity is increased by increasing kVp since low-energy photons might be more readily absorbed by metal than high-energy photons with higher penetration. Also, by raising the value of mAs,

the number of photons approaching the detector would maximize, minimizing noise and photon starvation. Decreasing collimation, the diameter of the detector would minimize scattering. The image quality can be improved with the use of an expanded Hounsfield unite (HU) and a soft filter reduces the appearance of metal artifacts [20]. Table 2.1 shows a variety of ways to minimize metal artifacts by modifying the acquisition, reconstruction, and visualization parameters. It further summarizes the benefits and drawbacks of the various steps taken.

Table 2.2: Benefits and drawbacks of adjusting acquisition, reconstruction, and visualization parameters in minimizing metal artifacts [9].

	Advantage	**Disadvantage**
Acquisition		
▪ Increase tube current (mAs)	▪ Reduced photon-starvation	▪ Increased radiation exposure
▪ Increase tube voltage (kVp)	▪ Increased photon penetration	▪ Decrease overall contrast
▪ Reduce total collimation i.e. the detector width	▪ Reduced scatter and partial volume averaging	▪ Increased scan time
▪ Lower pitch	▪ Reduced image noise	▪ Increased radiation exposure when mAs is not adapted
Reconstruction		
▪ Use of (model-based) iterative reconstruction techniques	▪ Reduced amplification of artifacts	▪ Computationally intensive, possible reduced spatial resolution
▪ Change from bone to soft reconstruction kernel	▪ Reduced visual conspicuity of metal artifacts	▪ Reduced spatial resolution
▪ Increase slice thickness	▪ Reduced image noise	▪ Partial volume artifacts
Visualization		
▪ Use of an extended	▪ Reduced visual conspicuity	▪ Limited availability and compatibility

Through transitioning to more modern iterative (IR) and model-based (MBIR) algorithms, we can use additional physical data, which helps to reduce both scatter and edge effects utilizing correction algorithms [9]. Using this process, metal artifacts are minimized and the image quality enhances. A study by Boudabbous et al. (2014) showed an 83% reduction of metal artifact size with MBIR relative to FBP in 62 patients [16]. MBIR minimized metal artifacts and thus provided an equivalent or greater visualization of the bone-metal

interfaces, and also a clearer evaluation of the soft tissue across the metal implants. The volume of the artifacts was minimized, and the subjective image quality was enhanced.

2.2.2 Manipulating Projection Data and/or Image Data

2.2.2.1 General Overview for MAR Algorithms

The starting point of MAR techniques was first defined by Kalender in 1987, who suggested an averaging or interpolation approach of adjacent detector components to substitute the affected projection results induced by metal influence [9]. To achieving this, CT or sinogram projection data is used to generate the incorrect image [9]. By thresholding, a metal image is eventually formed by assigning any pixels with a greater value as a metal image. The metal image is projected forward and coupled with the initial sinogram to create a metal sinogram. Back-projecting the uncorrected sinogram produces a corrected image that can be used as an input for more corrections. While this method decreases metal artifacts, it may also introduce new artifacts related to thresholding constraints, resulting in an inaccurate new sinogramv[9]. By utilizing a former image without artifacts, adding new artifacts may be minimized. To produce non-metal and metal images, a previous image is generated by thresholding an uncorrected image, with thresholds match up soft tissue, air, and bone tissue. The initial sinogram pixel values being separated by the sinogram of the previous image to obtain the standard sinogram and normalize it, which results in uniform pixel values just outside of the metal path. This leads to better reproduction of the metal by in-painting or linear interpolation [9]. Meyer et al. (2009) demonstrated that As Normalized Metal Artefact Reduction (NMAR) process is applied after de-normalization, the image can be generated by using filtered back-projection and inserting a metal image [25].

2.3 Previous Study

Subhas et al. (2018) studied lesions detectability close to hardware metal utilizing MBIR coupled with MAR software against FBP at decreased low dose level in a phantom experiment and reported that dose reduction did not compromise the accuracy compared to FBP. They also found that MBIR with MAR was considerably more effective than FBP in detecting small lesions and lesions close to the metal artifacts [9].

In a subsequent study [26], FBP against IMAR images of 40 shoulder patients and 21 hip patients were compared preoperatively and postoperatively. IMAR images were more accurate and fewer streaking artifacts compared to non-IMAR data.

In a spinal implants study, Kotsenas et al. (2015) and Aissa et al. (2017) found that IMAR enhanced the visualization of essential soft tissue around the implants [27,28]. Extreme artifacts caused by dental amalgam hardware and other hardware in the head and neck area have been minimized by IMAR [29,30].

Li et al. (2012) tested the application of O-MAR algorithm on a 16-slice CT scanner for phantom radiotherapy and 10 patients with hip implants[21]. CT numbers accuracy increased and noise decreased, particularly in a bilateral hip prosthesis, and the overall image quality and clarity of vital organs were substantially improved in O-MAR images relative to traditional images. Hilgers et al. (2014) also observed that the precision of CT numbers was higher for O-MAR compared to non-OMAR reconstructions in radiotherapy planning [31].

Teixeira et al. (2014) studied iterative reconstruction in 24 unilaterally and bilateral hip patients with and without the use of SEMAR. As SEMAR was paired with IR, the overall image quality improved showing obturator internus muscle, prostate or uterus, and bladder in high clarity. The MAR strategy proved to be effective in decreasing the amount of metal artifact [9]. These findings were confirmed by Yasaka et al. (2016), who studied 28 patients with metal hip prostheses, and Sonoda et al. (2015), who studied SEMAR and its utility in 58 patients with hip prostheses and embolization coils. SEMAR has no major effects on dental implants [32].

In patients with dental implants or fillings, O-MAR images lowered noise and increased CT number precision relative to non-O-MAR images [33]. Besides, higher consistency ratings have been reached in the streak of image artifacts concerning sharpness, texture naturalness, and degree of representation.

Boomsma et al. (2016) and Wellenberg et al. (2016, 2017) quantified the importance of O-MAR for total hip arthroplasty imaging utilizing a total hip arthroplasty phantom [9]. Applying IMR instead of iterative and traditional reconstruction improved overall image quality. The integration of IMR and O-MAR using 140 kVp led to a major increase in overall image quality and the most efficient artifact reduction with better CT number precision, lower noise values, and higher SNRs and CNRs [9]. Also, the IMR permitted an 80% reduction in radiation dose as the precision of the CT number was retained with lower noise levels and higher SNRs and CNRs [9].

A THA phantom study showed that the integration of IMR and O-MAR made it possible to reduce the radiation dose by 83 % where CT number precision, SNRs, and CNRs improved and noise decreased relative to the integration of iDose^4 and O-MAR [9].

de Kuya et al. (2017) reported that MBIR further decreases the size of artifacts and that MBIR enables for an equivalent or greater visibility of the bone-metal interface and increases the evaluation of soft tissue around implants relative to FBP [18]. Yasaka et al. (2013) as well observed that streak artifacts had been decreased using MBIR [17].

Bolstad et al. (2018) investigated MAR technology from the four major manufacturers. All strategies minimized metal artifacts and although various reconstruction kernels were used, the result was most apparent for SEMAR compared to IMAR, O-MAR, and SMAR and for stainless steel and cobalt-chromium implants compared to titanium implants [34].

A phantom study performed on a 64-slice CT scanner found that O-MAR greatly decreases metal artifacts using the iDose^4 partial iterative reconstruction technique. The iterative model-based reconstruction algorithm takes data statistics, image statistics, and machine models into account to generate an image that efficiently represents attenuation distributions [35].

Recent studies have shown that model-based iterative reconstruction techniques can decrease image noise close to 75%-83% and radiation dose approximately 75%-80% compared to traditional reconstruction techniques. Further developments in reconstruction algorithms, such as IMR, can further boost the efficacy of metal artifact reduction [35]. Recently, in a phantom study, O-MAR showed a significant decrease in metal artifacts when integrated with iDose^4 and IMR. Accuracy of CT numbers, SNRs, and CNRs were significantly improved, whereas noise values were reduced [9].

Chapter 3

Materials and Methods

This chapter provides the experimental framework of the study, from phantom design to the study design, image acquisitions, reconstructions, and data analysis.

3.1 Pelvis Phantom and Prosthesis

The phantom was planned and developed in the present study, which has a width of 380 mm, a height of 320 mm, and a depth of 250 mm and is made of polymethyl methacrylate (PMMA). The pelvis phantom with dimensions 30 x 27 x 15 cm has four major components, pelvis bones, muscle, fat, and vascular structures were fabricated as shown in Figure 3.1. The bony structures, soft tissue surrounding the pelvis, and vascular structures are produced by using different chemical materials with different concentrations as appears in Table 3.1. These materials were selected to resemble the human pelvis while still being compatible with CT imaging [36]. Furthermore, these materials have good elasticity with no loss of strength, and they are immune to bacterial contamination due to their low modulus [36].

After many trials to find out the correct material's percentage, the bony structure was created by using a plastic mold, with an internal mixture of 26 %weight calcium sulfate (CaSo4) combined with 74% weight water, and then the plastic mold was removed. For muscle tissue, the 3% weight of UltraPure™ agarose powder (UltraPure™ agarose; Sigma-Aldrich, St Louis, MO) was mixed with 97% weight water, the solution was heated to a temperature of 110-140°C then we added 2 ml of contrast media (Omnipaque™ (iohexol) 350 mg) to the mixture until the gel was formed. After that, the mixture was cold to 90°C. To achieve this percentage, 75 grams of agarose was mixed with 2500 ml of water. For Fat tissue, the bee wax with 89%weight was added to 11% weight of water by using 2500gram of bee wax which was mixed with 288gram of water. The mixture was heated to 60-65°C until the solution was formed then cold to 50°C. For vascular structures (external and internal common iliac, superficial and deep femoral arteries) were used the different diameters of extension tubes 9 mm, 5 mm, 8 mm, and 5 mm respectively. These tubes were filled with a 3% weight of contrast media (Omnipaque™ (iohexol) 350 mg) to ensure the optimal and required vascular enhancement in the arteries without making any streak effect on the phantom. Also, 2.6% weight of etherified hydroxyethylcellulose (Shin Etsu Tylose R HS

100000 YP2) and 0.2% weight of benzalkonium chloride (StepanguatR 50 NF) was used as an antibacterial agent. Additionally, CT number tests were done for these structures, to ensure mimicking the human pelvis density, representing CT number values of 900, 26, -90, and 400 for bone, muscle tissue, fat and vascular structures respectively.

Table 3.2: Material components of pelvis bone, soft tissue, and vessels.

Tissue	Component	Concentration
Bone	Plastic & calcium sulfate ($CaSo_4$)	26% $CaSo_4$ + 74% water
Fat	Bee wax & water	89% bee wax + 11% water
Muscle	Agarose powder & water	3% agarose powder + 97% water + 2 ml iohexol
Vascular structures	Iohexol + water	3% Iohexol + 97 water

Two types of the hip prosthesis were inserted in both femurs, the first one is a 40 mm head Metal on cemented cup total hip prosthesis, standard neck (Biomet Ltd, Waterton Industrial Estate, Bridgend, South Glamorgan CF 31 3XA, UK) was inserted with a titanium-aluminum-vanadium (Ti-6Al-4V) stem in the left femur. The second one is a 46 mm head metal on metal Austen Moore (Excel Stainless Steel, Standard Stem, NARANG medical Ltd) was used for the right femur. The justification of using two types of the hip prosthesis is that both total hip and Austen Moore prostheses are widely used in certain countries for the management of femoral neck fractures not only in young but also in older patients [4].

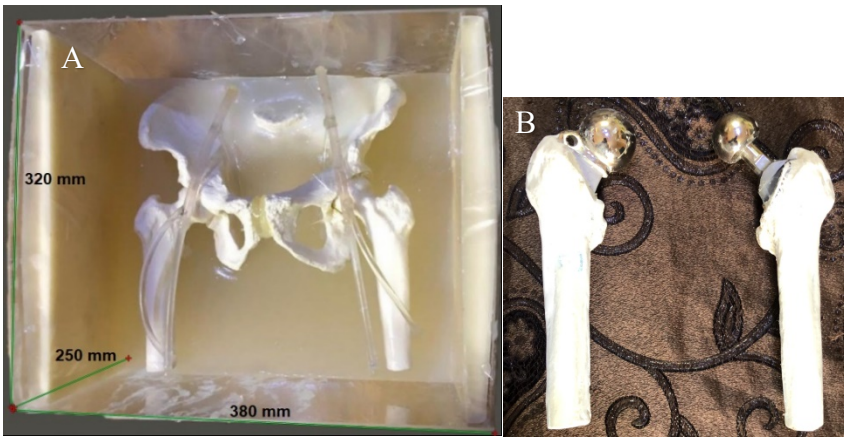

Figure 3. 3: (A) The pelvis phantom with dimensions. The phantom used was made of polymethyl methacrylate (PMMA) containing bone, soft tissue, fat and vascular structures. (B) Two types of hip prosthesis were inserted in both femurs, a 40 mm head Metal on cemented cup total hip prosthesis, the standard neck was inserted with a titanium-aluminum-vanadium (Ti-6Al-4V) stem in the left femur. For the right femur, a 46 mm head metal on metal Austen Moore was used.

3.2 Study Design, Image Acquisitions, and Reconstructions

Phantom scans were obtained first without the insertion of two types of the hip prosthesis, then two days later the scans with the prosthesis were carried out. All images without and with the prosthesis were obtained with FBP and reconstructed using iDose[4], and IMR, and also with and without O-MAR, for a more detailed description of O-MAR we refer to "Appendix A", and evaluated using a consistent analysis template mask. Scans without and with the prosthesis were acquired at low, (two-standard) [37] and high-dose CT-dose index (CTDI) of 12.0, 28, 28.5, and 30.0 miliGray (mGy) at 80, 100, 120, and 140 kVp respectively producing 8 different acquisitions. Dose modulation was on during scans without the prosthesis and was off with the prosthesis scans. Milliampere-seconds (mAs) values without and with the prosthesis were the same but different for each kVp setting. mAs values were (390 – 550), (340 – 420), (293 – 387) and (261 – 356) respectively for 80, 100, 120, and 140 kVp settings. However, the scan of CTDI at 28.5 mGy at 120 kVp reconstructed with FBP without a prosthesis was the standard protocol on the CT machine. The designed phantom was scanned using a Philips Brilliance iCT 128-slice CT-scanner (Cleveland, OH), where reading from the acquisitions without adding the prosthesis was used as a reference value. Fixed scan parameters were 64 × 0.625 mm collimation, 1.5 mm slice thickness with 1.0

mm increment, 460 mm field of view, 0.524 pitch, 512 × 512 image matrix, 0.5s rotation time, and value of 60 and 360 for window level and window width respectively were used in our study.

The IMR reconstruction system (version R11) was used. For traditional, iterative, and model-based iterative reconstruction, noise reduction levels and filter forms were adapted. The iDose^4 from Philips can reduce noise at seven different levels. we use iDose^4 level 4 because this is the middle level of noise reduction for iDose^4, also for reasonable contrast the middle level of Philips' IMR, level 2, was selected. iDose^4, a fourth-generation hybrid IR algorithm, and model-based iterative reconstruction algorithm (IMR), a full iterative reconstruction technique, both are introduced by Philips Healthcare (Cleveland, OH), for a more thorough overview of iDose^4 and IMR algorithms, see "Appendix B and Appendix C". The choice of the soft and the sharper reconstruction kernels were made based on the kernels that are commonly used in the hospital's clinic for CT examinations in the pelvic area. In CT imaging of metal materials, a strong or sharp filter was selected to improve contrast and reinforce edges between hard and soft objects. As a consequence, the sharp filter D has been used for iDose^4 and FBP, while the IMR filter Sharp Plus was used.

3.3 Data Analysis

3.3.1 Quantitative Analysis

Different regions of interest (ROIs) are analyzed and evaluated by measuring CT numbers in the Hounsfield unit (HU), noise levels, and SNRs to assess image quality, as well as the severity of metal artifacts and the efficacy of metal artifact reduction. To increase the reliability of the measurements, a standardized measurement prototype mask was used for each scan. Scan measurements were made using a precise measuring layout to improve the scan's reliability. The axial slice was exactly centered in the study regions and, and stored as a Digital Imaging and Communications in Medicine (DICOM) file for each of the 36 datasets. A single axial slice was inserted in ImageJ version 2.64, and the five ROIs (R1 - R5) prototype was generated manually as shown in Figure 3.2. The five RIOs representing the following anatomy (right common iliac artery, left common iliac artery, right gluteus medius muscle, fat, and ubladder) respectively from R1 – R5.

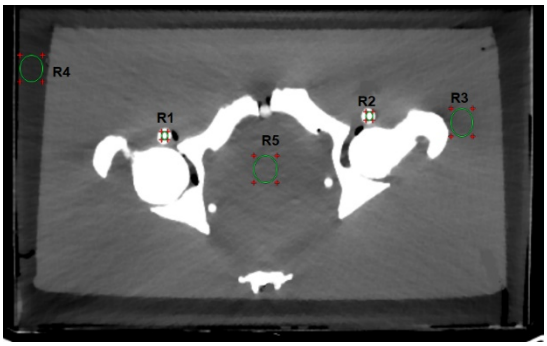

Figure 3.4: Axial CT-slice acquired at 120-kVp with IMR. Also, it shows the measurement template mask including the ROIs of the 5 regions (R1-R5).

Real quantitative analyses were performed using MATLAB® 2014b. Regions (R3 - R5) had a diameter of 360 pixels or 2.60 cm and (R1 and R2) had a diameter of 30 pixels or 0.24 cm which minimizing partial volume effects in all regions and ensuring that regions (R3 and R5) are at the middle of the artifact. The standard deviation of the pixels in an ROI was used to determine the noise level, with and without the insertion of a prosthesis. SNRs were determined by splitting CT numbers measurements of ROIs from the noise level or standard deviation. Metal artifact correction via O-MAR was determined for CT numbers, noise levels, and SNRs as follows [35]:

$$\text{Deviation}_{\text{without O-MAR}} = |\text{reference value - value without O-MAR}| \quad (1)$$

$$\text{Deviation}_{\text{with O-MAR}} = |\text{reference value - value with O-MAR}| \quad (2)$$

$$\text{Correction}_{\text{by O-MAR}}\ (\%) = \left(1 - \left(\frac{\text{Deviation with O-MAR}}{\text{Deviation without O-MAR}}\right)\right) \times 100 \quad (3)$$

3.3.2 Statistical Analysis

For the statistical manipulation of our data; both descriptive and inferential statistical methods are used with a focus on the descriptive approach. The statistical analysis was carried out using the Minitab® statistical software. On one hand, descriptive statistical methods such as percentages, means, and charts were suggested by the nature and goals of our study where we compared the performance of different algorithms under different conditions and assumptions. On the other hand, when we consider the five regions of interest collectively, along with all four levels of energy it became reasonable (to a good degree) to conduct inferential parametric statistics where we utilized the t-test comparing two independent population means with unknown and possibly unequal population standard

deviations. This tool of analysis will be used on a larger scale with our future studies. A value of $p < 0.05$ was used as a significance standard.

Chapter 4

Results and Discussion

This chapter outlines the results of the study, the effect of using O-MAR, IMR, and integration of O-MAR and IMR in correction and improvement on CT numbers, noise, and SNRs values without and with the insertion of the prosthesis, with a discussion of the results.

4.1 Without the Insertion of the Prosthesis

IMR resulted in lower reference CT number values in comparison with FBP and iDose^4 for regions R1-R5 as shown in Table 4.1. Also, IMR resulted in lower noise values compared to FBP and iDose^4 ($p<0.001$) and increased SNRs in comparison with FBP and iDose^4 ($p<0.05$) for all regions.

Table 4.3: Reference values of CT numbers, noise values, and SNRs for regions R1-R5 at 80, 100, 120, and 140-kVp reconstructed with FBP, iDose^4, and IMR.

		FBP				**IDOSE^4**				**IMR**				
	kVp	**80**	**100**	**120**	**140**	**80**	**100**	**120**	**140**	**80**	**100**	**120**	**140**	*p*-value
CT NUMBER (HU)	**R1**	666	621	578	495	649	589	546	470	605	576	466	357	0.38
	R2	754	671	547	474	615	601	522	460	601	554	422	366	
	R3	41	33	27	27	33	30	27	25	26	25	23	22	
	R4	-100	-99	-88	-75	-93	-86	-76	-61	-88	-75	-67	-55	
	R5	45	39	38	28	34	30	26	26	28	26	25	25	
NOISE	**R1**	43	40	37	30	30	27	23	18	18	13	9	6	<0.001
	R2	48	42	34	28	27	27	23	20	19	16	11	6	
	R3	36	29	23	22	21	18	16	13	6	5	5	4	
	R4	40	34	28	23	20	16	12	10	7	5	4	4	
	R5	36	27	25	15	15	13	11	10	6	5	4	4	
SNRS	**R1**	15.5	15.5	15.6	16.3	21.6	21.8	23.7	25.8	33.9	43.8	52.2	61.5	<0.05
	R2	15.7	15.9	16.2	16.7	22.7	22.7	23	23	31.9	35.7	40.3	58.2	
	R3	1.1	1.2	1.2	1.2	1.6	1.7	1.7	2	4.3	5	5	5.2	
	R4	2.5	2.9	3.1	3.2	4.6	5.3	6.2	6.2	12.2	15	15.2	15.3	
	R5	1.2	1.4	1.5	1.9	2.3	2.4	2.4	2.6	4.4	5.3	6	6.1	

CT number, noise values, and SNRs showed little variation at similar kVps settings (Table 4.2). Using IMR, CT number values at kVps of 80, 100, 120, and 140 were respectively 11%, 10%, 14%, and 14% lower compared to iDose^4 and respectively 24%, 20%, 23%, and 18% lower compared to FBP without any significant changes ($p>0.05$).

Table 4.4: Reduction of CT numbers and noise values, and improvement of SNRs for R1-R5 at 80, 100, 120, and 140-kVp reconstructed with FBP, iDose^4, and IMR.

		CT number Reduction %		**Noise Reduction %**		**SNRs Improvement %**	
	kVp	**IMR vs. FBP**	**IMR vs. iDose^4**	**IMR vs. FBP**	**IMR vs. iDose^4**	**IMR vs. FBP**	**IMR vs. iDose^4**
R1	**80**	9.16	6.81	58.06	40	1.18	0.56
R2		20.27	2.35	60.71	30.41	1.03	0.4
R3		37.1	21.9	83.51	71.92	2.81	1.78
R4		12.17	5.07	82	64	3.88	1.64
R5		38.82	18.95	82.57	57.37	2.51	0.9
R1	**100**	7.24	2.24	67.46	51.82	1.82	1.01
R2		17.36	7.75	63.18	41.36	1.24	0.57
R3		24.47	16.52	82.4	71.8	3.29	1.96
R4		25.03	12.81	85.29	69.14	4.1	1.82
R5		32.76	11.31	81.56	60.29	2.65	1.23
R1	**120**	22.82	18.3	75.71	60.87	2.35	1.2
R2		22.87	19.16	68.94	53.98	1.48	0.76
R3		15.32	14.18	80.04	71.04	3.24	1.96
R4		24.06	12.43	84.29	64.52	3.83	1.47
R5		32.53	3.86	83.1	61.34	2.99	1.49
R1	**140**	27.98	24.11	80.2	67.03	2.76	1.38
R2		22.8	20.5	77.91	68.59	2.49	1.53
R3		15.86	11.76	80.41	65.54	3.3	1.56
R4		11.53	9.84	84.35	63.27	3.71	1.47
R5		11.82	4.5	72.97	59.53	2.26	1.36
Average %		22.34 ± 9	12.22 ± 7	76.73 ± 9	59.69 ± 11	2.65 ± 1	1.30 ± 0.5
p-value		0.31	0.38	<0.05	<0.05	<0.05	<0.05

Using IMR, noise levels at kVps of 80, 100, 120 and 140 were respectively 53%, 59%, 62% and 65% lower compared to iDose^4 and respectively 73%, 76%, 78% and 79% lower compared to FBP ($p<0.05$). Using IMR, at kVps of 80, 100, 120, and 140, SNRs were a factor 1, 1.32, 1.38, and 1.46 higher compared to iDose^4 and a factor 2.3, 2.7, 2.8, and 2.9 higher compared to FBP ($p<0.05$).

4.2 With the Insertion of the Prosthesis

Four regions of interest R1, R2, R3, and R5 of the hip phantom were affected by the prosthesis located on the bilateral side. Therefore, we only focused on these regions as shown in Figure 4.1. The most affected region of interest was region R5 located between the two prosthesis heads. Region R4 (unaffected), regions R2 and R3 (moderate artifacts), located near the prosthesis head, and region R5 (severe artifacts) were further evaluated and selected based on visual assessment. Also, R1 was analyzed because it appears to be influenced by a white streak artifact on the medial and upper sides of the prosthesis head. Both regions R1 and R5 were the primary focusing of this study.

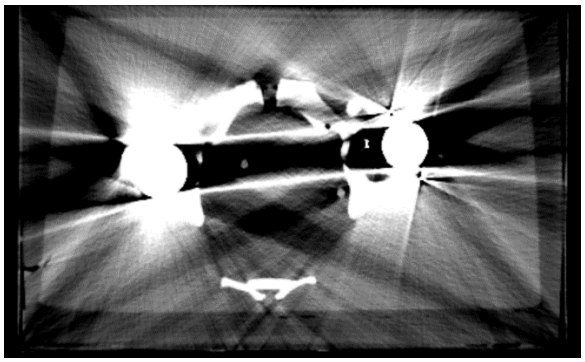

Figure 4.1: A 120-kVp acquisition reconstructed with iDose^4 level 4 and without the use of O-MAR. Region R5 located between the two heads prosthesis is invisible due to severe metal artifacts. Region R1 seems to be affected by a white streak artifact.

4.2.1 CT Numbers

Figure 4.2 displays the deviated CT numbers, noise, and SNRs for regions R1, R2, R3, R4, and R5 using FBP at 120 kVp and the standard dose. Without using O-MAR, SNRs decreased and noise values increased compared to reference values due to metal artifacts for all regions. Also, CT number values decreased for regions R3 and R5 but increased for regions R1 and R2 because they were affected by white streak artifacts. The usage of O-MAR reduces CT number variations in regions R1, R2, R3, and R5 from baseline values and was most noted in regions R1 and R5. Region R4 was unaffected by metal artifacts since it was beyond the prosthesis's axial scan area. CT numbers of region R4 were equivalent with and without the application of O-MAR, confirming the statement that O-MAR would not work in areas free of metallic artifacts.

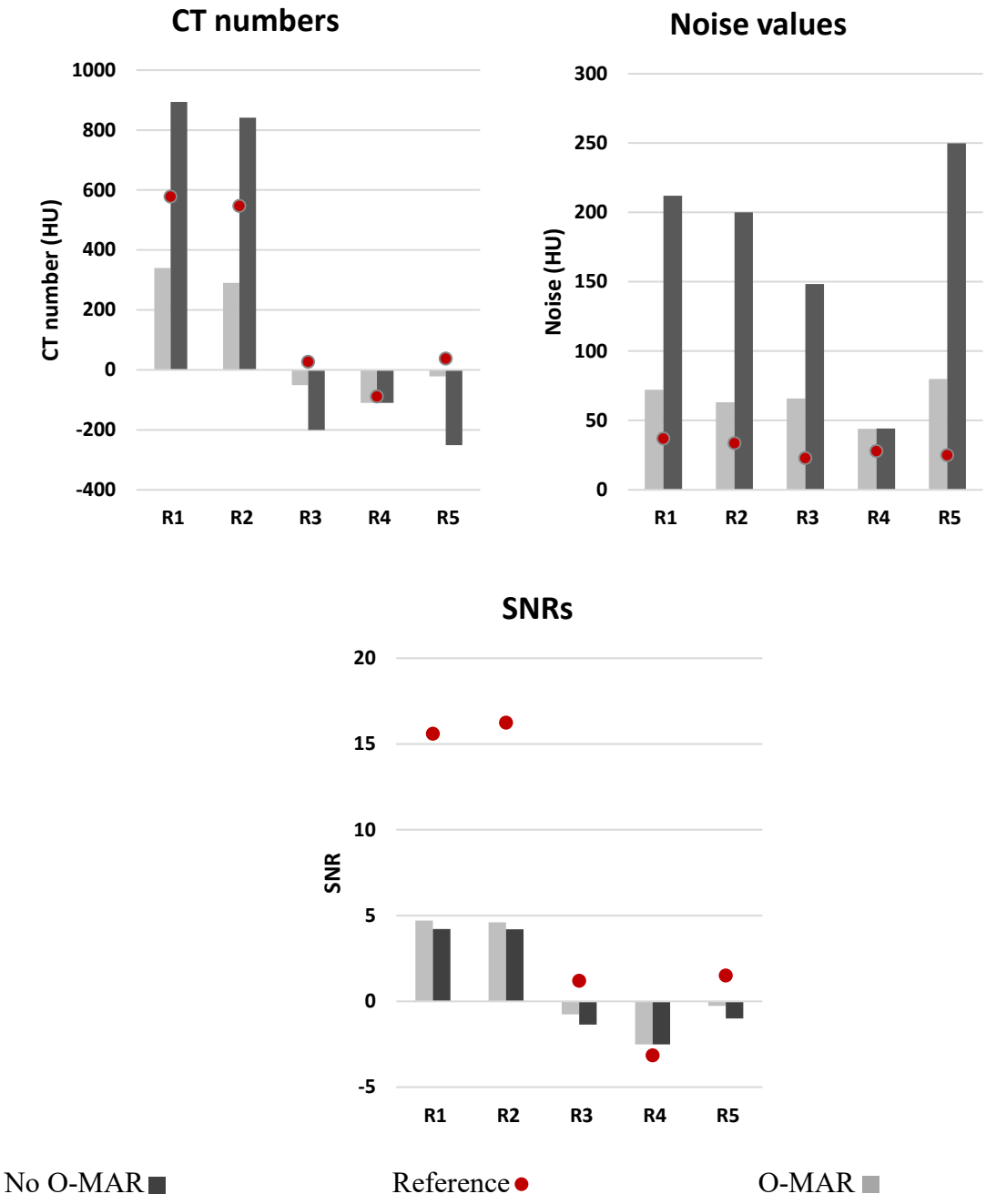

Figure 4.2: CT numbers, noise values, and SNRs for regions R1, R2, R3, R4, and R5 at 120-kVp reconstructed with FBP after prosthesis insertion. The reference values are shown in red in the absence of the prosthesis.

The influence of O-MAR in conjunction with the various reconstruction techniques is shown in Figure 4.3. We explored the impact of O-MAR in conjunction with FBP, iDose^4, and IMR, concentrating on the most severe metal artifacts in regions R1 and R5. Regions R1 and R5 are highly influenced by severe metal artifacts due to the large metal head and cannot be visualized without O-MAR for all reconstruction techniques as shown in Figure 4.3 (A, B, and C). Using O-MAR, region R1 can be visualized but only when paired with IMR. Also, when O-MAR is paired with iDose^4 or IMR region R5, it is possible to see it again. O-MAR suppresses artifacts and renders all these regions visible again when paired with iDose^4 or IMR. O-MAR has no impact on the unaffected region R4 and is most useful in treating the most severe artifacts in the case of regions R1 and R5 as shown in Figure 4.3 (D, E, and F).

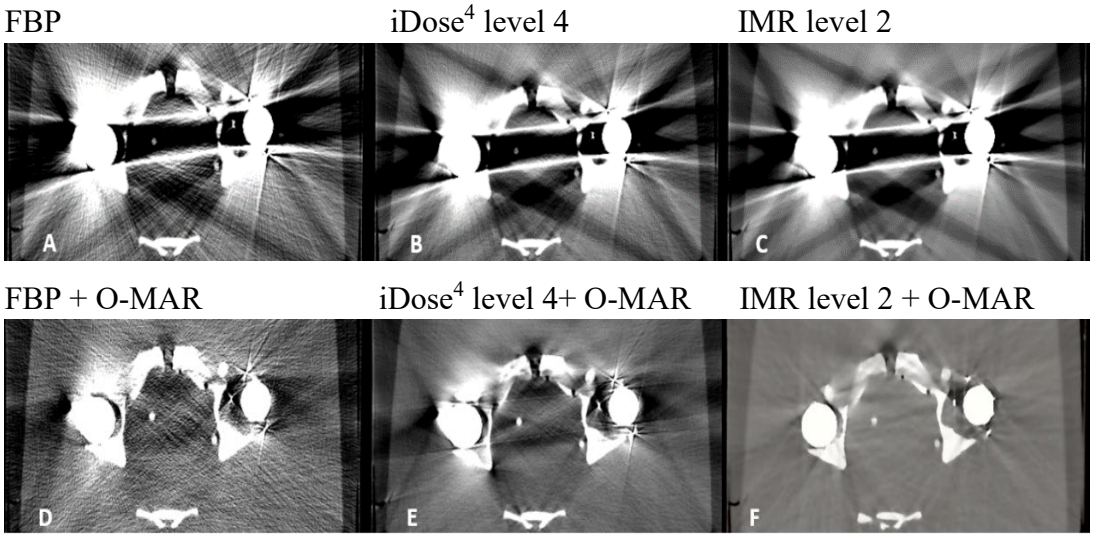

Figure 4.3: 140-kVp standard-dose images reconstructed with FBP, iDose^4, and IMR and with and without the use of O-MAR. (A): the reconstructed images obtained with FBP, (B): the reconstructed images obtained with iDose^4, (C): the reconstructed images obtained with IMR, (D): the images reconstructed with O-MAR combined with FBP, (E): the images reconstructed with O-MAR combined with iDose^4, (F): the images reconstructed with O-MAR combined with IMR.

Region R1, O-MAR improved CT-number precision by 49% and 83% for respectively for FBP, IMR ($p<0.05$), compared to iDose^4 by 57% without any significant changes ($p>0.05$) (Figure 4.4, Table 4.3).

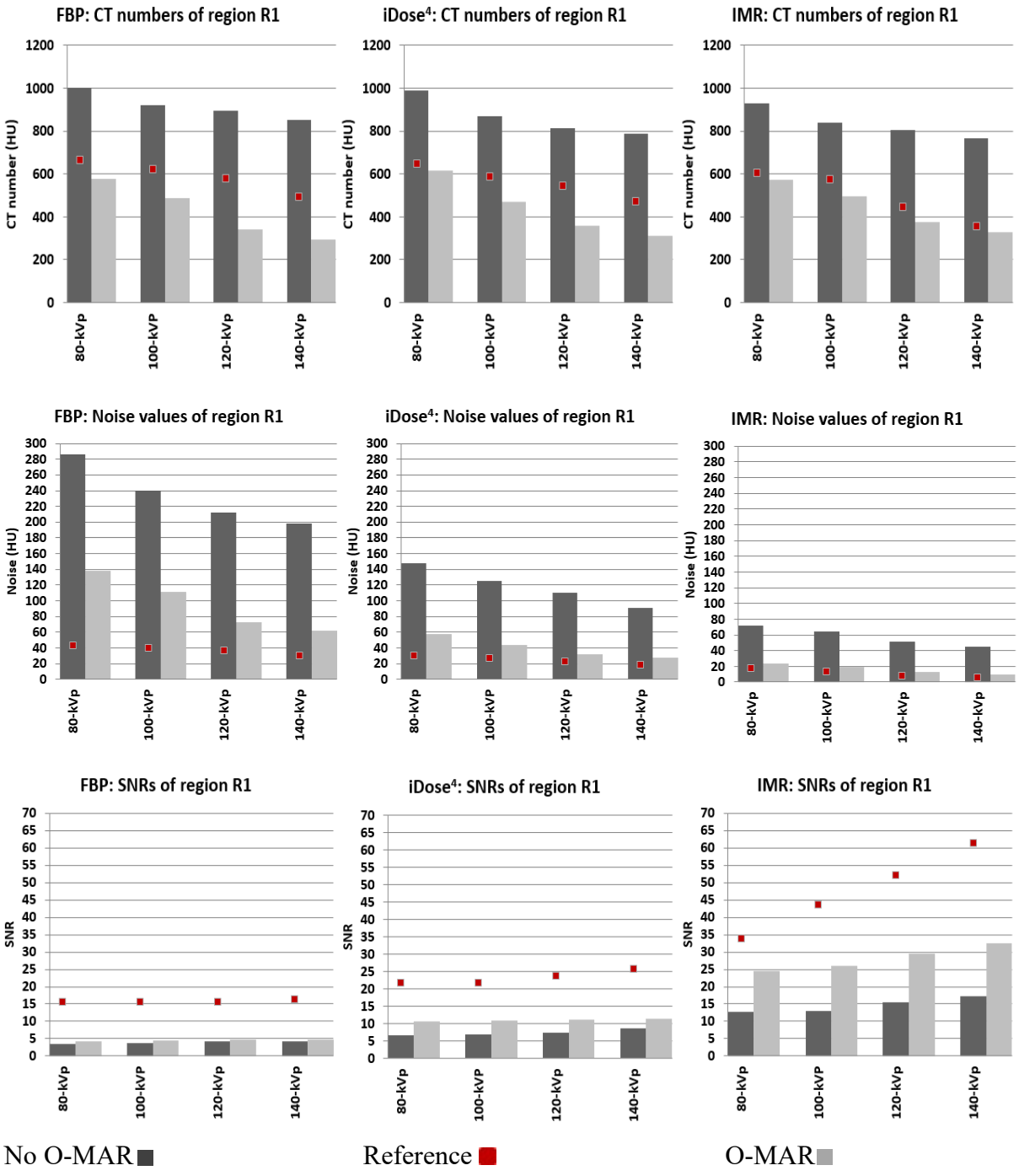

Figure 4.2: CT numbers, noise values, and SNRs in severe metal artifacts in region R1 at 80, 100, 120, and 140-kVp utilizing FBP, iDose^4, and IMR. The reference values are shown in red in the absence of the prosthesis.

Table 4.3: Corrections in CT-numbers, noise values, and SNRs of region R1 by application of O-MAR to reference values utilizing FBP, iDose^4, and IMR for the 4 different acquisitions.

	HU (%)			Noise (%)			SNR (%)		
kVp	**FBP**	**iDose^4**	**IMR**	**FBP**	**iDose^4**	**IMR**	**FBP**	**iDose^4**	**IMR**
80	73	89	90	60	76	89	6	26	55
100	56	58	68	64	83	88	5	26	42
120	25	30	81	80	89	90	4	23	38
140	43	49	93	81	87	89	4	16	34
Average (%)	49 ± 20	57 ± 24	83 ± 11	71 ± 11	84 ± 6	89 ± 1	5 ± 1	23 ± 5	42 ± 9
p-value	<0.05	0.06	<0.05	<0.05	0.06	<0.05	<0.05	<0.05	<0.05

In the case of the most severe artifacts in region R5, O-MAR improved CT-number precision by 81%, 89%, and 92% against baseline values for respectively FBP, iDose^{4,} and IMR ($p<0.05$) (Figure 4.5, Table 4.4).

Table 4.4: Corrections in CT-numbers, noise values, and SNRs of region R5 by application of O-MAR to reference values utilizing FBP, iDose^4, and IMR for the 4 different acquisitions.

	HU (%)			Noise (%)			SNR (%)		
kVp	**FBP**	**iDose^4**	**IMR**	**FBP**	**iDose^4**	**IMR**	**FBP**	**iDose^4**	**IMR**
80	79	87	90	79	90	92	28	32	37
100	80	89	90	78	89	91	29	36	38
120	80	90	93	76	91	92	30	38	46
140	84	90	93	83	91	92	27	42	52
Average (%)	81 ± 2	89 ± 1	92 ± 2	79 ± 3	90 ± 1	92 ± 0.5	29 ± 1	37 ± 4	43 **± 7**
p-value	<0.05	<0.05	<0.05	<0.05	<0.05	<0.05	<0.05	0.09	<0.05

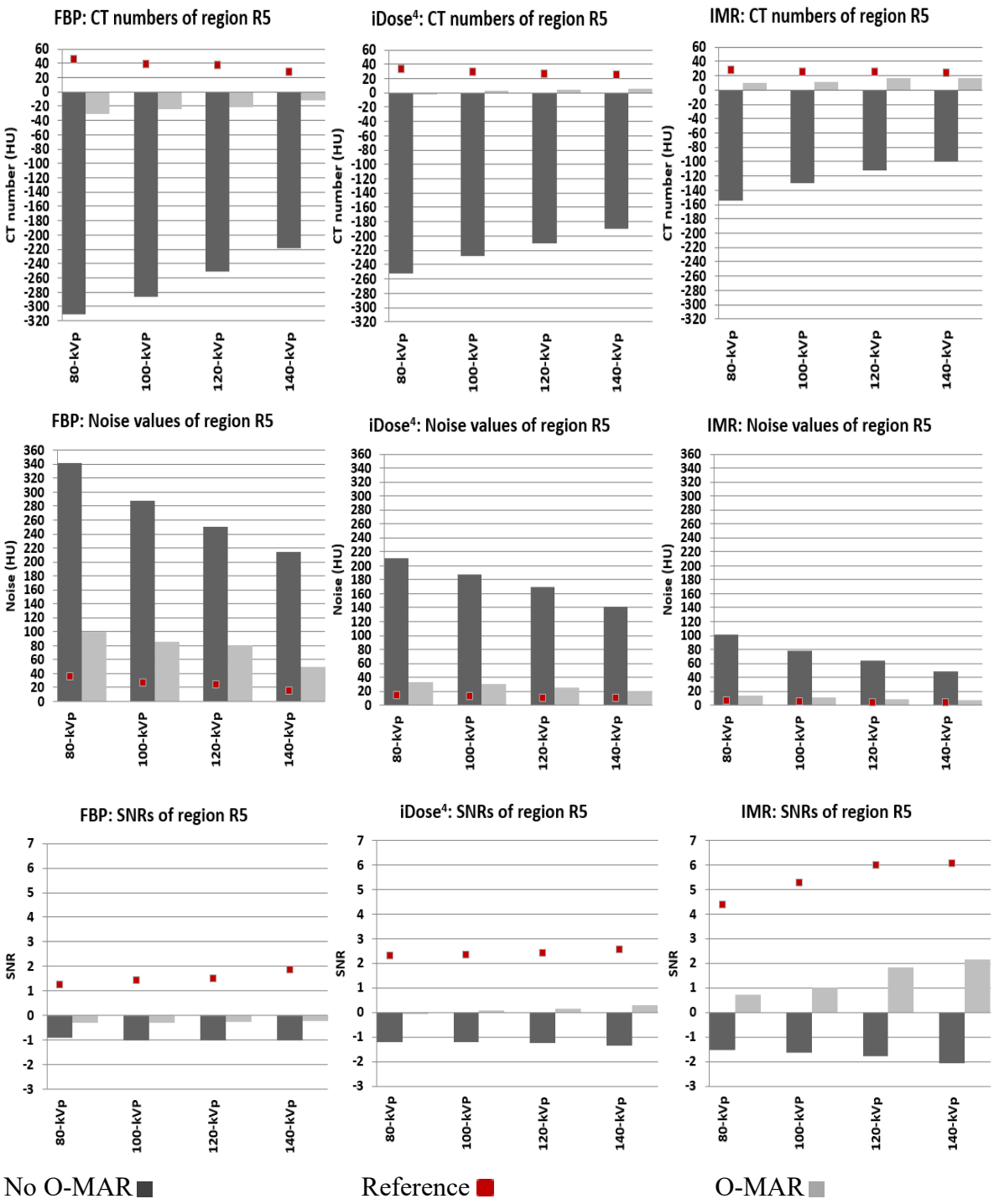

Figure 4.5: CT numbers, noise values, and SNRs in severe metal artifacts in region R5 at 80, 100, 120, and 140-kVp utilizing FBP, iDose^4, and IMR. The reference values are shown in red in the absence of the prosthesis.

4.2.2 Noise Values

The standard deviation of pixels in the ROIs has been used to quantify the noise of the ROIs. Metal artifacts increased noise values by elevating standard deviation in all regions and particularly in regions R1 and R5 (Figure 4.2). Noise values of region R4 were slightly higher than reference values without the insertion of the prosthesis. O-MAR can minimize noise values when paired with FBP, iDose^4, and IMR. Because IMR images had relatively lower noise values, O-MAR was most successful in treating noise when IMR was implemented, with corrections in the noise in region R1 by 71% and 89% for respectively for FBP and IMR ($p<0.05$), compared to iDose^4 by 84% without any significant changes ($p>0.05$) (Figure 4.4, Table 4.3). For region R5 with the most severe artifacts, O-MAR reduced noise values by 79 %, 90 %, and 92 % for respectively FBP, iDose^4, and IMR ($p<0.05$) (Figure 4.5, Table 4.4).

4.2.3 SNRs

O-MAR had a good impact concerning HU correction in regions R2 and R3 with greater HU correction by O-MAR for regions R1 and R5, although the HU values of region R4 stayed fairly stable as shown in Figure 4.2. Although O-MAR did not enhance CT numbers of all affected regions to reference values in the absence of a prosthesis, SNRs increased significantly for other regions besides regions R1 and R5 (Figure 4.2). SNRs of region R5 were negative, obliterating the boundary between region R5 and the adjacent tissue (Figure 4.3(A-C)). On the other hand, SNRs of region R1 were positive but less than the reference value without insertion of the prosthesis, eliminating the boundaries across the region R1, since it was affected by white streak artifact (Figure 4.3(A-E)).

O-MAR was most successful in enhancing overall SNR and makes all these regions clear again when paired with iDose^4 or IMR (Figure 4.3(A-C)). Overall SNR was significantly higher for IMR images and O-MAR became more successful in correcting SNR deviations when paired with IMR with total SNR corrections region R1 by 5 ± 1, 23 ± 5, and 42 ± 9 for respectively FBP, iDose^4, and IMR ($p<0.05$) (Figure 4.4, Table 4.3). O-MAR greatly enhances SNR corrections among the most severe artifacts in region R5 with 29 ± 1 and 43 ± 4 for respectively FBP and IMR ($p<0.05$), compared to iDose^4 by 37 ± 7 without any significant changes at ($p<0.05$) (Figure 4.5, Table 4.4). Although O-MAR was unable

to return SNRs to reference values of unaffected regions R4, a great visual improvement was observed when paired with IMR as shown in Figure 4.2.

When paired with IMR and for 140-kVp performance, O-MAR found to be most successful in cases of the most severe artifacts in regions R5 (Table 4.4). For region R5, O-MAR paired with IMR revealed an average HU correction of 90%, 90%, 93%, and 93% for respectively 80, 100, 120, and 140-kVp results. Noise was corrected for with 92%, 91%, 92% and 92% for respectively 80, 100, 120 and 140-kVp results. SNR corrections were 37%, 38%, 46% and 52% for respectively 80, 100, 120 and 140-kVp results. On the other hand, for region R1, O-MAR efficiency showed little variation when paired with IMR and for 80 and 140-kVp results regarding SNRs (Table 4.3). O-MAR paired with IMR yielded an average HU correction of 90%, 68%, 81%, and 93% for respectively 80, 100, 120, and 140-kVp results. Noise was corrected with 89%, 88%, 90% and 89% for respectively 80, 100, 120 and 140-kVp results. SNR corrections were 55%, 42%, 38% and 34% for respectively 80, 100, 120 and 140-kVp results.

4.4 Discussion

At all-tube voltages, our results indicate that iterative model-based reconstruction (IMR) significantly decreases noise value relative to traditional FBP and iterative reconstruction approaches (iDose^4) ($p<0.001$). Besides, IMR enhances image quality with higher SNRs than FPB and iDose^4 ($p<0.05$). The justification behind these findings is that model-based iterative reconstruction approaches can handle the increased detector noise levels especially at lower doses better than traditional reconstruction techniques such as FBP and iterative reconstruction techniques as they combine data statistics, image statistics, and system models [9].

IMR had lower CT numbers relative to FBP and iDose^4. This can be demonstrated by variations in kernel kind, while filter D was used for FBP and iDose^4 and Sharp Plus have been used for IMR. The Sharp kernel utilizes edge enhancement at structure interfaces, which may affect edge enhancement at the interfaces between structures, which may affect CT numbers in a small region of interest or small structures [38].

Metal artifacts are represented as deviations from the (unaffected) mean CT numbers in HU, noise [HU], and SNRs [9]. O-MAR decreases metal artifacts and is most powerful in the case of severe artifacts in region R5, and when paired with IMR dependent on corrections in deviated HU values ($p<0.05$), and noise values ($p<0.05$), although SNRs did not show any significant improvement ($p>0.05$). While the integration of O-MAR and IMR in region R1 resulted in a significant correction in deviated SNRs ($p<0.05$), there was no significant improvement in noise or HU values ($p>0.05$). While the integration of O-MAR and IMR in region R1 resulted in a significant correction in deviated SNRs ($p<0.05$), there was no significant improvement in noise or HU values ($p>0.05$).

We realized that integrating O-MAR and (model-based) iterative reconstruction improves image quality. That's because the O-MAR algorithm post-processes the projection data and delivers more consistent attenuation profiles until image reconstruction. These consistent attenuation profiles have the potential to increase the overall efficiency of iDose^4 and IMR [46]. A study by de Kuya et al. (2017) stated that MBIR further reduces the size of the artifacts and that allows for an equal or better visibility of the bone-metal interface and improves the assessment of soft tissue around the implant compared to FBP [18]. Yasaka et al. (2013) also found that the use of MBIR had reduced streak artifacts, leading to an improved overall image quality [17].

Concerning HU values, O-MAR had a good impact on intermediate artifacts with slight HU differences in most cases. This impact was observed for regions R2 and R3. CT numbers, noise values, and SNRs of region R4 verified that O-MAR would not change the data in regions not influenced by metal artifacts [22]. A study by Boomsma, M. F. et al. (2016), stated that unaffected area by metal artifact helps for more precise bone mineral density measurements in CT in the acetabular region, which may be used in THA surgical repair [39]. At all reconstruction algorithms and tube voltages, O-MAR reduced HU differences in severe metal artifacts influencing region R5 ($p<0.05$). In most instances, O-MAR minimized noise and increased SNRs in other impacted regions. O-MAR revealed regions R1 and R5 in all cases once reconstructed with iDose^4 or IMR, demonstrating variations in O-MAR efficacy when paired with (model-based) iterative reconstruction approaches. According to a previous study, IMR increases overall image quality, and O-MAR is most successful in severe artifacts and when paired with IMR in enhancing CT number precision, SNRs, and CNRs while also reducing noise [20]. This can be explained by O-MAR ability to detects and

replaces projections that crossed through metal with interpolated data from neighboring projections that did not [48]. Besides, image noise potentially could be eliminated with IMR, which would create an artifact- and noise-free image [43].

Using FBP, the total noise values were high and slightly decreased even with O-MAR because FBP itself cannot actually manage the noise, and particularly in severe artifacts [9]. Mainly, the artifact's geometry and structure were similar by utilizing FBP, IMR, and iDose^4 with and without application of O-MAR. However, we found noticeable variations in image quality through a significant reduction in noise in region R5 by utilizing iDose^4 and IMR.

Typically, as tube voltage is lowered noise rises. The integration of IMR and O-MAR contributes to better noise reduction than iDose^4 and FBP at 80 kVp in our findings for regions R5 and R1. The explanation for this finding is that IMR is more able to manage elevated detector noise levels compared as it integrates data statistics, image statistics, and device models. Also, O-MAR has shown usefulness even in lower tube voltages, due to specific metal separation and tissue segmentation at low tube voltages [46]. A study by Boomsma et al. (2015) [41] used iDose^4 to measure the significance of O-MAR by adjusting multiple scan parameters. They reported that although iDose^4 has little impact on the results of O-MAR, it could assist in imaging at a lower dose due to improvements in CNRs. They noticed that O-MAR is effective in reducing severe artifacts by 32% relying on CT numbers utilizing iDose^4, while we found that O-MAR would lead to HU correction by 89% utilizing iDose^4 and 92% using IMR. Also, related to previous studies [44,45], we found that IMR reduced noise significantly at low tube voltage and helped improve image quality relative to FPB. The findings of our research indicate that noise is reduced when IMR is applied in low-dose acquisition. which is important to minimize the dose in clinical practice as well. A side effect of this excessive noise reduction in low-dose acquisitions may result in image blurring, resolution degradation, and over-smoothing of the image [42]. However, It is best to be cautious when decreasing the dosage since there is a smoothing impact, which results in the lack of tiny details and low-contrast detectability [9]. There could be more variation and uncertainty in the measured noise levels than what can be expected due to just doing a single scan of any of the different situations.

Also, we found that using the combination of IMR and O-MAR with 120 and 140-kVp were successful in MAR with lower noise and better SNR in case of severe metal artifact in region R5. The use of a higher tube voltage of 140-kVp that penetrates metal with higher-energy x-ray beams could support O-MAR in the reduction of metal artifacts and noise correction [51]. Although using a tube voltage of 140 kVp will increase the radiation dose up to 30 mGy, it remains within the permissible limit [51]. Moreover, O-MAR resulting in more consistent attenuation profiles before image reconstruction, potentially improving the overall efficiency of IMR [20]. A Previous study stated that the integration of IMR and O-MAR with 140 kVp led to a major increase in overall image quality and the most efficient in reducing artifacts with better CT number precision, lower noise levels, and improved SNRs [9]. Research by Wellenberg et al. [35] showed that minimizing severe metal artifacts with O-MAR with improving CT number precision by 50%, 60%, and 63%, and reducing noise by 1%, 62%, and 85% whereas improving SNRs by 27%, 47%, and 46% and with FBP, iDose^4 and IMR respectively, where we found improving CT number accuracy by 81%, 89%, and 92% and reducing noise by 79%, 90% and 92% whereas improving SNRs by 29%, 37%, and 43% and with FBP, iDose^4, and IMR respectively. A potential reason for the reported variations may be that they have used a different measurement template, different CT scanner, water uses rather than soft tissue material around the phantom, use of a unilateral total hip prosthesis, different slice thickness, and the use of a different filter type.

Numerous metal artifact suppression strategies were shown to greatly enhance the overall image quality while reducing artifacts with increased diagnostic confidence as described earlier. Many studies observed that O-MAR led to a better CT number precision and lowered noise values [40,33,21] as O-MAR is an iterative projection adjustment approach that identifies and corrects data distorted by streak artifacts using uncorrupted projection data [48]. Nevertheless, no analysis into the added utility of the O-MAR has been conducted to see whether it works along with model-based iterative reconstruction. Related results on CT numbers precision and noise reduction were seen in other O-MAR studies [42,35,33]. While using O-MAR, a voltage of 140 kVp is recommended in case of severe metal artifacts caused by the beam-hardening effect, as a result of lower deviations in CT numbers, noise levels, and SNRs relative to reference values. Also, at a 140-kVp setting, both beam-hardening and the statistical noise are reduced, which supports the O-MAR algorithm [22]. Latest studies indicate that MBIR approaches have reduced image noise to around 75% and 83%, and radiation dose by 75% - 80%, compared to traditional reconstruction approaches [35].

IMR has displayed greater image quality and improved diagnostic precision relative to FBP and iDose[4]. Region R1 has greatly improved SNRs through the O-MAR and utilizing IMR algorithm relative to FBP and iDose[4] ($p<0.05$). Since O-MAR is effective at low tube voltage [46], we noticed the reverse effect of O-MAR when coupled with IMR at low tube voltage at 80-kVp compared with 140-kVp on SNRs. Relative SNRs improvement by O-MAR was the highest in the acquisition of 80-kVp for IMR reconstruction with 55% higher than 140-kVp with 34 %. There are some benefits to the reduction of kVp setting. It has been recommended that employing an 80–100 kVp rather than a 120-140 kVp is an important means for greater contrast enhancement [47]. Also, reducing the kVp setting boost vascular enhancement. The intrinsic attenuation of iodine-based contrast agents increases with decreased X-ray peak energy toward the K-edge energy of 33.2 Kilo Electron Volts (keV) due to the high relative atomic number of iodine [47]. An analysis by Fan Zhang et al. revealed that using 80 kVp together with IMR may have significant benefits in enhancing overall image quality [43]. This finding is probably due to IMR's ability to boost low- and high-contrast detectability by reducing image noise and artifacts, as well as the use of 80 kVp protocols to enhance the vascular structure.

Chapter 5

This chapter shows the conclusion of the study, limitations, recommendations, and future studies.

5.1 Conclusion

O-MAR decreases the appearance of metal artifacts using partial iterative reconstruction technique iDose^4 and is most efficient in severe artifacts when used in combination with 140-kVp and IMR. O-MAR has shown usefulness even in lower tube voltages. O-MAR would not change the data in regions not influenced by metal artifacts. IMR provides better image quality compared to FBP and iDose^4. In the CT imaging of a bilateral total hip prosthesis phantom, using IMR together with O-MAR increases image quality by significantly minimizing metal artifacts, reducing noise, and enhancing CT number and SNR. This would support the diagnosis of soft tissue lesions, bone disease, and vascular defects in patients with bilateral hip prostheses.

5.2 Limitations

There are certain limitations to our research. We just conducted quantitative methods. More subjective image quality evaluation may offer more insight into the practical utility and added value of CT strategies. The rectangular form of the phantom with sharp edges might be replaced with an oval shape showing more natural human pelvic dimensions. To measure metal artifacts, the standard deviation of pixels in an ROI was used to calculate the noise. We are conscious that both noise and artifacts can influence an ROI's standard deviation, and that it is hard to tell which is more influential.

Regardless of the fact where CT numbers, noise, and SNRs are appropriate and regularly used image quality criteria, further measurements of the contrast to noise ratios (CNRs), modulation transfer function (MTF) and noise power spectrum (NPS) will provide more information about the nature of the noise.

5.3 Recommendations

1. In the case of metal prostheses, post-processing algorithms such as (iDose^4, IMR, and O-MAR) can minimize metal artifacts much better than conventional acquisition and reconstruction.

2. The ideal option for a significant reduction in severe metal artifacts caused by beam hardening and improved image quality is to use 140-kVp, O-MAR, and IMR.

3. Since O-MAR works at low tube voltages, using the acquisition of 80 kVp with a combination of IMR and O-MAR is an important means for greater contrast enhancement and boost vascular structure.

4. When using IMR with O-MAR at low tube voltages, be cautious because the smoothing effect can result in a loss of small information and low-contrast detectability.

5. There is no need to use O-MAR if there is no metal in the scanning field of view as it has no impact on enhancing image quality.

6. Continuous education for physicians, radiologists, and radiographers about the dangers and advantages of CT-dose, as well as how to optimize CT-dose in the case of a metal prosthesis.

5.4 Future Studies

More experiments and studies on this phantom should be conducted at various CTDIvol values to determine the best degree of hybrid and model-based iterative reconstruction algorithms for reducing metal artifacts in CT imaging while enhancing overall image quality and lowering the patient dose. A multi-vendor compression analysis should also be done to assess the effectiveness of various commercial metal artifact reduction technology and reconstruction techniques. Finally, standard low dose protocol should be adjusted in case of a metal artifact to provide the diagnostic image with less radiation dose.

References

1. Blum, A., J. B. Meyer, A. Raymond, M. Louis, O. Bakour, R. Kechidi, A. Chanson & P. Gondim-Teixeira CT of hip prosthesis: New techniques and new paradigms. Diagn. Interv. Imaging 97, 725–733 (2016).
2. Lahham, A., Kameel, S., Jerusalem, E. & Jerusalem, E. Estimation of Female Radiation Doses and Breast. Am. J. Roentgenol. 179, 1–7 (2018).
3. Arjah, H., Hjouj, M. & Hjouj, F. Low dose brain CT, comparative study with brain post processing algorithm. ACM Int. Conf. Proceeding Ser. 1–7 (2019).
4. Bazzocchi, A., Bartoloni, A., Rimondi, E., Albisinni, U. & Guglielmi, G. Imaging After Hip Joint Replacement Surgery in the Elderly Population. Curr. Radiol. Rep. 5, 1–14 (2017).
5. Katsura, M., Sato, J., Akahane, M., Kunimatsu, A. & Abe, O. Current and novel techniques for metal artifact reduction at CT: Practical guide for radiologists. Radiographics 38, 450–461 (2018).
6. Boas, F. E. & Fleischmann, D. CT artifacts: Causes and reduction techniques. Imaging Med. 4, 229–240 (2012).
7. Yadava, G. K., Pal, D. & Hsieh, J. Reduction of metal artifacts: beam hardening and photon starvation effects. Phys. Med. Imaging 9033, 1679–1691 (2014).
8. Lee, Mi Jung, Sungjun Kim, Sung Ah Lee, Ho Taek Song, Yong Min Huh & Dae Hong Kim. Overcoming artifacts from metallic orthopedic implants at high-field-strength MR imaging and multidetector CT. Radiographics 27, 791–803 (2007).
9. Wellenberg, Ruud H.H., Martijn F. Boomsma, Jochen A.C. van Osch, Alain Vlassenbroek, Julien Milles, Mireille A Edens &Geert J. Reducing metal artefacts and radiation dose in musculoskeletal CT imaging. Journal of Computer Assisted Tomography vol. 40 (University of Amisterdam, 2018).
10. Andersson, K. M., Nowik, P., Persliden, J., Thunberg, P. & Norrman, E. Metal artefact reduction in CT imaging of hip prostheses-an evaluation of commercial techniques provided by four vendors. Br. J. Radiol. 88, 1–7 (2015).
11. NV, K. P. E. iDose^4 Iterative Reconstruction Technique. Breakthrough in image Quality and Dose Reduction With the 4th Generation of Reconstruction. Eindhoven: Philips Healthcare (2011).
12. Joemai, R. M. S., De Bruin, P. W., Veldkamp, W. J. H. & Geleijns, J. Metal artifact reduction for CT: Development, implementation, and clinical comparison of a generic and a scanner-specific technique. Med. Phys. 39, 1125–1132 (2012).
13. Kardell, M. Automatic Segmentation of Tissues in CT Images of the Pelvic Region. (Linköping University, 2014).
14. Geyer, Lucas L., U. Joseph Schoepf, Felix G. Meinel, John W. Nance, Gorka Bastarrika & Jonathon A. Leipsic. State of the Art: Iterative CT reconstruction techniques. Radiology 276, 339–357 (2015).
15. Arapakis I, Efstathopoulos E, Tsitsia V, Kordolaimi S, Economopoulos N, Argentos S. et al. Using " iDose ^{4} " iterative reconstruction algorithm in adults ' chest – abdomen – pelvis CT examinations : effect on image quality in relation to patient radiation exposure. Br. Inst. Radiol. 87, 2–8 (2014).

16. Boudabbous, Sana, Daniel Arditi, Emilie Paulin, Aphrodite Syrogiannopoulou, Christoph Becker & Xavier Montet. Model-based iterative reconstruction (MBIR) for the reduction of metal artifacts on ct. Am. J. Roentgenol. 205, 380–385 (2015).

17. Yasaka, Koichiro, Masaki Katsura, Masaaki Akahane, Jiro Sato, Izuru Matsuda & Kuni Ohtomo. Model-based iterative reconstruction for reduction of radiation dose in abdominopelvic CT: Comparison to adaptive statistical iterative reconstruction. Springerplus 2, 1–9 (2013).

18. Kuya, Keita, Yuki Shinohara, Ayumi Kato, Makoto Sakamoto, Masamichi Kurosaki & Toshihide Ogawa. Reduction of metal artifacts due to dental hardware in computed tomography angiography: assessment of the utility of model-based iterative reconstruction. Neuroradiology 59, 231–235 (2017).

19. Mehta, D, R Thompson, T Morton, A Dhanantwari, E Shefer & Philips Healthcare. I Iterative model reconstruction: simultaneously lowered computed tomography radiation dose and improved image quality. Med. Phys. Int. J. 1–9 (2013).

20. Wellenberg, R. H.H., M. F. Boomsma, J. A.C. van Osch, A. Vlassenbroek, J. Milles, M. A. Edens, G. J. Streekstra, C. H. Slump & M. Maas. Low-dose CT imaging of a total hip arthroplasty phantom using model-based iterative reconstruction and orthopedic metal artifact reduction. Skeletal Radiol. 46, 623–632 (2017).

21. Li, Hua, Camille Noel, Haijian Chen, H. Harold Li, Daniel Low, Kevin Moore, Paul Klahr. et al. Clinical evaluation of a commercial orthopedic metal artifact reduction tool for CT simulations in radiation therapy. Med. Phys. 39, 7507–7517 (2012).

22. Philips CT Clinical Science. Metal Artifact Reduction for Orthopedic Implants (O-MAR). Philips Healthc. 1–12 (2012).

23. Roth, T. D., Maertz, N. A., Andrew Parr, J., Buckwalter, K. A. & Choplin, R. H. CT of the hip prosthesis: Appearance of components, fixation, and complications. Radiographics 32, 1089–1107 (2012).

24. Gjesteby, Lars, Bruno De Man, Yannan Jin, Harald Paganetti, Joost Verburg, Drosoula Giantsoudi & Ge Wang. Metal Artifact Reduction in CT: Where Are We After Four Decades. IEEE Access 4, 5826–5849 (2016).

25. Meyer, E., Raupach, R., Lell, M., Schmidt, B. & Kachelrieß, M. Normalized metal artifact reduction (NMAR) in computed tomography. Med. Phys. 37, 5482–5493 (2010).

26. Subhas, Naveen, Joshua M. Polster, Nancy A. Obuchowski, Andrew N. Primak, Frank F. Dong, Brian R. Herts & Joseph P. Iannotti. Imaging of arthroplasties: Improved image quality and lesion detection with iterative metal artifact reduction, a new CT metal artifact reduction technique. Am. J. Roentgenol. 207, 378–385 (2016).

27. Kotsenas, A. L., G. J. Michalak, D. R. DeLone, F. E. Diehn, K. Grant, A. F. Halaweish, A. Krauss. et al. CT metal artifact reduction in the spine: Can an iterative reconstruction technique improve visualization? Am. J. Neuroradiol. 36, 2184–2190 (2015).

28. Aissa, J. Thomas, L. M. Sawicki, J. Caspers, P. Kröpil, G. Antoch & J. Boos. Iterative metal artefact reduction in CT: can dedicated algorithms improve image quality after spinal instrumentation? Clin. Radiol. 72, 428.e7-428.e12 (2017).

29. Weiß, Jakob, Christoph Schabel, Malte Bongers, Rainer Raupach, Stephan Clasen, Mike Notohamiprodjo, Konstantin Nikolaou & Fabian Bamberg. Impact of iterative

metal artifact reduction on diagnostic image quality in patients with dental hardware. Acta radiol. 58, 279–285 (2017).

30. Diehn, Felix E, Gregory J Michalak, David R DeLone, Amy L Kotsenas, E Paul Lindell, Norbert G Campeau, Ahmed F Halaweish, Cynthia H McCollough & Joel G Fletcher. CT Dental Artifact: Comparison of an Iterative Metal Artifact Reduction Technique with Weighted Filtered Back-Projection. Acta Radiol. Open 6, 205846011774327 (2017).

31. Hilgers, G., Nuver, T. & Minken, A. The CT number accuracy of a novel commercial metal artifact reduction algorithm for large orthopedic implants. J. Appl. Clin. Med. Phys. 15, 274–278 (2014).

32. Yasaka, Koichiro, Kouhei Kamiya, Ryusuke Irie, Eriko Maeda, Jiro Sato & Kuni Ohtomo. Metal artefact reduction for patients with metallic dental fillings in helical neck computed tomography: Comparison of adaptive iterative dose reduction 3D (AIDR 3D), forward-projected modelbased iterative reconstruction solution (FIRST) and AIDR 3D with. Dentomaxillofacial Radiol. 45, 1–7 (2016).

33. Kidoh, M., T. Nakaura, S. Nakamura, S. Tokuyasu, H. Osakabe, K. Harada & Y. Yamashita. Reduction of dental metallic artefacts in CT: Value of a newly developed algorithm for metal artefact reduction (O-MAR). Clin. Radiol. 69, e11–e16 (2014).

34. Bolstad, K., Flatabø, S., Aadnevik, D., Dalehaug, I. & Vetti, N. Metal artifact reduction in CT, a phantom study: subjective and objective evaluation of four commercial metal artifact reduction algorithms when used on three different orthopedic metal implants. Acta radiol. 59, 1110–1118 (2018).

35. Wellenberg, Ruud H.H., Martijn F. Boomsma, Jochen A.C. Van Osch, Alain Vlassenbroek, Julien Milles, Mireille A. Edens, Geert J. Streekstra, Cornelis H. Slump & Mario Maas. Computed tomography imaging of a hip prosthesis using iterativemodel-based reconstruction and orthopaedicmetal artefact reduction: A quantitative analysis. J. Comput. Assist. Tomogr. 40, 971–978 (2016).

36. Makhamrah, O., Ahmad, M. S. & Hjouj, M. Evaluation of liver phantom for testing of the detectability multimodal for hepatocellular carcinoma. ACM Int. Conf. Proceeding Ser. 17–21 (2019).

37. Horehledova, Barbora, Casper Mihl, Gianluca Milanese, Rutger Brans, Nienke G. Eijsvoogel, Babs M.F. Hendriks, Joachim E. Wildberger & Marco Das. CT Angiography in the Lower Extremity Peripheral Artery Disease Feasibility of an Ultra-Low Volume Contrast Media Protocol. Cardiovasc. Intervent. Radiol. 41, 1751–1764 (2018).

38. Narita, A. & Ohkubo, M. A pitfall of using the circular-edge technique with image averaging for spatial resolution measurement in iteratively reconstructed CT images. J. Appl. Clin. Med. Phys. 21, 144–151 (2020).

39. Boomsma, Martijn F., Inge Slouwerhof, Christiaan Van Lingen, Dean F.M. Pakvis, Jorn A. Van Dalen, Mireille A. Edens, Harmen B. Ettema, Cees C.P.M. Verheyen & Mario Maas.. CT-based quantification of bone stock in large head metal-on-metal unilateral total hip replacements. Eur. J. Radiol. 85, 760–763 (2016).

40. Huang, essie Y., James R. Kerns, Jessica L. Nute, Xinming Liu, Peter A. Balter, Francesco C. Stingo, David S. Followill, Dragan Mirkovic, Rebecca M. Howell & Stephen F. Kry. An evaluation of three commercially available metal artifact

reduction methods for CT imaging. Phys. Med. Biol. 60, 1047–1067 (2015).

41. Boomsma, Martijn F., Inge Slouwerhof, Jorn A. van Dalen, Mireille A. Edens, Dirk Mueller, Julien Milles & Mario Maas. Use of internal references for assessing CT density measurements of the pelvis as replacement for use of an external phantom. Skeletal Radiol. 44, 1597–1602 (2015).

42. Wellenberg, Ruud H.H., Jochen A.C. van Osch, Henk J. Boelhouwers, Mireille A. Edens, Geert J. Streekstra, Harmen B. Ettema & Martijn F. Boomsma. CT radiation dose reduction in patients with total hip arthroplasties using model-based iterative reconstruction and orthopaedic metal artefact reduction. Skeletal Radiol. 48, 1775–1785 (2019).

43. Zhang, Fan, Li Yang, Xiang Song, Ying Na Li, Yan Jiang, Xing Hua Zhang, Hai Yue Ju, Jian Wu & Rui Ping Chang. Feasibility study of low tube voltage (80 kVp) coronary CT angiography combined with contrast medium reduction using iterative model reconstruction (IMR) on standard BMI patients. Br. J. Radiol. 89, (2016).

44. Yuki, Hideaki, Daisuke Utsunomiya, Yoshinori Funama, Shinichi Tokuyasu, Tomohiro Namimoto, Toshinori Hirai, Ryo Itatani, Kazuhiro Katahira, Shuichi Oshima & Yasuyuki Yamashita. Value of knowledge-based iterative model reconstruction in low-kV 256-slice coronary CT angiography. J. Cardiovasc. Comput. Tomogr. 8, 115–123 (2014).

45. Oda, S., Weissman, G., Vembar, M. & Weigold, W. G. Iterative model reconstruction: Improved image quality of low-tube-voltage prospective ECG-gated coronary CT angiography images at 256-slice CT. Eur. J. Radiol. 83, 1408–1415 (2014).

46. Hu, Yi, Shinong Pan, Xudong Zhao, Wenli Guo, Ming He & Qiyong Guo. Value and clinical application of orthopedic metal artifact reduction algorithm in CT scans after orthopedic metal implantation. Korean J. Radiol. 18, 526–535 (2017).

47. Matsuoka, Shin, Andetta R. Hunsaker, Ritu R. Gill, Isabel B. Oliva, Beatrice Trotman-Dickenson, Francine L. Jacobson & Hiroto Hatabu. Vascular enhancement and image quality of MDCT pulmonary angiography in 400 cases: Comparison of standard and low kilovoltage settings. Am. J. Roentgenol. 192, 1651–1656 (2009).

48. Boomsma, Martijn F., Niek Warringa, Mireille A. Edens, Dirk Mueller, Harmen B. Ettema, Cees C.P.M. Verheyen & Mario Maas. Quantitative analysis of orthopedic metal artefact reduction in 64-slice computed tomography scans in large head metal-on-metal total hip replacement, a phantom study. Springerplus 5, 1–10 (2016).

49. Arapakis, Efstathopoulos E, Tsitsia V, Kordolaimi S, Economopoulos N, Argentos S, et al. Using 'iDose^4' iterative reconstruction algorithm in adults' chest-abdomen-pelvis CT examinations: Effect on image quality in relation to patient radiation exposure. Br. J. Radiol. 87, 1–8 (2014).

50. Arjah, Hamza, Hjouj, M. Low Dose Brain CT, Comparative Study With Brain Post Processing Algorithm. (Al-Quds university, 2020).

51. Kesong Zhang, MMa, PhDa , Qing Han, MMb , Xiaolin Xu, MMc . et al. Metal artifact reduction of orthopedics metal artifact reduction algorithm in total hip and knee arthroplasty. Medicine (Baltimore). 99, 8 (2020).

تقييم تطبيق خوارزميات الحد من التشويه الناتج عن الزرعات المعدنية العظمية وإعادة البناء التكراري في التصوير المقطعي المحوسب للأطراف الاصطناعية للورك.

الملخص

يتسبب تصوير CT للأطراف الاصطناعية للورك المعدني في حدوث عيوب بالصورة تقلل من جودة الصورة الإجمالية والقيمة التشخيصية لجهاز CT. الهدف من هذه الدراسة هو التقييم الكمي لاستخدام خوارزميات الحد من التشويه الناتج عن الزرعات المعدنية العظمية (O-MAR) وإعادة البناء التكراري المستند إلى النموذج (IMR) في CT للأطراف الاصطناعية للورك في مجسم الحوض. مجسم الحوض يحتوي على أربع مكونات تشميل العظم، العضلات، الدهن والشرايين. وتم عملها باستخدام تركيزات مختلفة من كبريتات الكالسيوم، شمع العسل، مسحوق الاغاروز والايوهكسول. تم استخدام نوعين من الزرعات المعدنية تشمل الحوض الكلي وطرف اوستن مور. تم تطبيق أنواع مختلفة من الخوارزميات على المجسم تضمنت الإسقاط الخلفي المفلتر (FBP)، وإعادة الإعمار التكراري الهجين من الجيل الرابع (iDose^4) و (IMR) مع استخدام طاقات فولتية ذرية مختلفة (kVps) عند 80 و100 و120 و140 بالتزامن مع تطبيق O-MAR. تم تقييم جودة الصور باستخدام الإعدادات الرقمية التي تتمثل في قيمة Hounsfield unit (HU)، والتشويش، ونسبة الإشارة الى التشويش. ومن ثم تحليلها بواسطة خمس مناطق في مقطع عرضي واحد. حيث كانت المناطق ر1 و ر2 هي مناطق التركيز الأساسي. تمثل هذه المناطق التشريح التالي: (الشريان الحرقفي المشترك الأيمن، الشريان الحرقفي الأيسر المشترك، العضلة الألوية المتوسطة اليمنى، الدهون، والمثانة البولية) على التوالي من ر1 الى ر5. أظهرت النتائج أن IMR أدى الى تقليل قيم HU، نسبة التشويش وزيادة في SNRs مقارنة مع FBP وiDose4 لجميع المناطق في حال عدم وجود الطرف الصناعي. مع وجود الطرف الصناعي، حسنت خوارزمية O-MAR قيمة HU في المنطقة ر1 بنسبة 49٪ و83٪ على التوالي لكل من FBP وIMR والقيمة الاحتمالية (< 0.001)، مقارنة مع iDose^4 بنسبة 57٪. أما في المنطقة ر5، تحسنت قيمة HU نسبة 81٪ و89٪ و92٪ نحو قيم المرجع لكل من FBP و iDose4 و IMRعلى التوالي والقيمة الاحتمالية (< 0.05). أيضا O-MAR كان أكثر فاعلية في تقليل التشويش عند دمجه مع IMR في المنطقة ر5 بنسبة تصحيح 79٪ و90٪ و92٪ على التوالي لكل من FBP وiDose^4 وIMR والقيمة الاحتمالية (< 0.05). بالمقارنة في المنطقة ر1، قلت قيم التشويش بنسبة 71٪ و89٪ على التوالي لكل من FBP وIMR والقيمة الاحتمالية (< 5%)، مقارنة مع iDose^4 بنسبة 84 ٪. و كان O-MAR أكثر فاعلية في تصحيح انحرافات نسبة الإشارة الى التشويش عند دمجه مع IMR في المنطقة ر5 بنسبة 29 ± 1 و 43 ± 4 على التوالي لكل من FBP وIMR والقيمة الاحتمالية (< 0.05)، مقارنة مع iDose^4 بنسبة و 37 ± 7. وفي المنطقة ر1 كانت بمقدار 5 ± 1 و 23 ± 5 و 42 ± 9 على التوالي لكل من FBP و iDose^4 و IMR والقيمة الاحتمالية (< 5%). أثبت O-MAR فاعلية أكثر في تصحيح قيم HU عند دمجه مع IMR و نتائج 140-kVp. وكانت في المنطقة ر5 بنسبة 90٪ و 90٪ و 93٪ و 93٪ لنتائج 80 و 100 و 120 و 140 كيلو فولت على التوالي. وتم تصحيح التشويش بنسبة 92٪ و91٪ و92٪ و92٪ على التوالي لنتائج 80 و100 و120 و140 كيلو فولت على التوالي، وكانت تصحيحات نسبة الإشارة الى التشويش بنسبة 37٪ و38٪ و46٪ و52٪ لنتائج 80 و100 و120 و140 كيلو فولت على التوالي. لكن بالنسبة للمنطقة ر1، أظهرت كفاءة O-MAR اختلافًا طفيفًا عند دمجها مع IMR ونتائج 80 و140 كيلو فولت حيث

كان متوسط تصحيح HU فيلد بنسبة 90٪ و68٪ و81٪ و93٪ لنتائج 80 و100 و120 و140 كيلو فولت على التوالي. وتصحيح التشويش بنسبة 89٪ و88٪ و90٪ و89٪ على التوالي لنتائج 80 و100 و120 و140 كيلو فولت، وكانت تصحيحات نسبة الإشارة الى التشويش بنسبة55٪ و42٪ و38٪ و34٪ لنتائج 80 و100 و120 و140 كيلو فولت على التوالي. في الختام، يقلل O-MAR من ظهور العيوب المعدنية باستخدام iDose^4 ويكون أكثر فاعلية عند استخدامه مع 140 kVp وIMR. عمل CT للأطراف الاصطناعية باستخدام IMR مع O-MAR على زيادة جودة الصورة عن طريق تقليل التشويش، وتحسين HU ونسبة SNRs.

APPENDICES

APPENDIX A

Orthopedic Metal Artifact Reduction Algorithm

The commercial OMAR algorithm assessed in this study is an iterative projection adjustment approach [22]. (OMAR) algorithm made by Philips Health System, Cleveland, USA, and is used to erase metal artifacts through data acquisition modification. The O-MAR algorithm utilizes an iterative loop in which the metal sinogram is obtained and then acts as a mask to correct the calculated sinogram. The output correction image is subtracted from the source images. The resulting image then becomes a new input image and the step can be replicated. The first step is to set the threshold for producing a metal-only image in the source image. The metal-only image consists of all pixels set to zero, except those which are classified as metal. Metal data points in the sinogram are substituted by interpolated values that simulate tissue in place of metal. This sinogram is re-projected and the resulting image is used to segment tissue to build a tissue-classified image. This phase is not carried out for subsequent iterations. Over one or even more cycles, if there are no large clusters of metal pixels in the image, hence no processing is done and the final, corrected images are measured [48].

APPENDIX B

iDose is the 4th generation iterative reconstruction algorithm developed by Philips Healthcare (Cleveland, OH) used to avoid photon starvation artifacts (streaks, biases) after image formation and to preserve image texture. iDose^4 involves iterative modeling in both projection and image domains. In the projection domain, the algorithm determines and corrects the noisiest values, those with very low SNRs, or very low photon counts. By using a model that contains actual photon statistics from each projection and iterative diffusion process, noisy data, underlying structures are maintained and spatial resolution is preserved thus allowing for considerable noise reduction. The next major component of the iDose^4 algorithm interacts with the subtraction of image noise by calculating the noise distribution in the image volume. This eliminates noise while maintaining the underlying edges consistent with real anatomy or pathology. After that, a selector distinguishes between the noiseless structural models, and the one that best matches the local image volume topology is selected. When the optimal model has been selected, it is used to decrease the noise in the image volume [49,50].

APPENDIX C

A model-based iterative reconstruction algorithm

Philips' MBIR-based iterative model-based reconstruction algorithm (IMR) is a complete iterative reconstruction technique. Improves the process of reconstruction by integrating device models and photon statistics [19]. With MBIR, images are being reconstructed at decreased levels of radiation at minimal levels of noise. In comparison, MBIR decreases the volume of artifacts and allows for equivalent or greater visualization of bone-metal interfaces, and facilitates the evaluation of soft tissue around implants relative to FBP [16]. IMR differs from FBP approaches in that the reconstruction process will be an adjustment strategy that involves data statistics, image statistics, and comprehensive CT machine geometry. Figure C.1 shows an overview of the IMR algorithm. This adjustment strategy can be limited by the cost function of (a) The variance between the calculation of the data and the real data obtained; (b) a concept of regularization. it can be assumed that a noisy image would be a reasonable solution to the reconstruction issue, which reduces the gap between the predicted and the real data, a restriction (regularization) is needed to obtain a better image. A restriction that hinders image noise would guide the adjustment strategy to generate noiseless images, and the level to which it is implemented could regulate the level of noise reduction. Such a restriction would consider the effects of knowledge of data statistical models (knowledge of quantum noise statistics in projection data) and could set limits to fix the problem. The achieved spatial resolution of the final image is guided by the sampling of the detector, angular sampling, and device geometry. Spatial resolution can be increased without the inclusion of image artifacts by using this information in the adjustment strategy. Compatible models for various device elements and system physics can be added. Together, a comprehensive review of the system properties enables the design of the cost feature, allowing IMR to efficiently monitor image noise while optimizing spatial resolution at radiation doses that are substantially smaller than those typically used for FBP reconstruction [19].

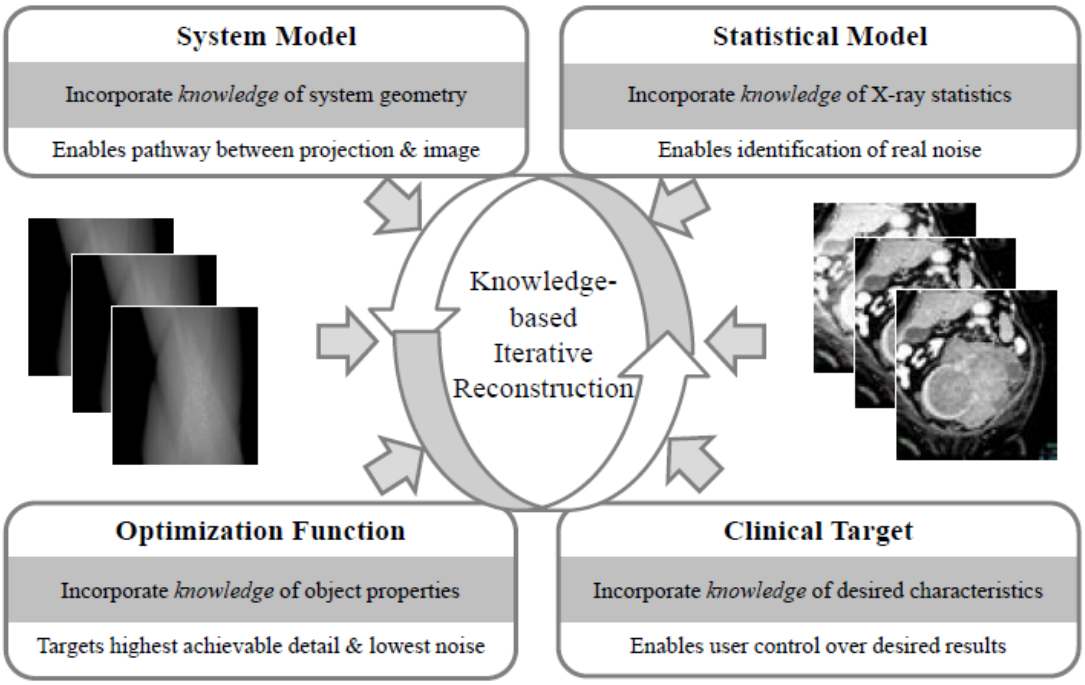

Figure C.2: IMR – Algorithm Overview [19].